# GADD34 mRNA turnover controls the molecular memory of cellular stress experience

Vera Magg[1], Alessandro Manetto[1], Katja Kopp[1], Julia Welsch[1], Lucy Eke[2], Stefan M. Kallenberger[3,4], Volker Haucke[5,6], Nicolas Locker[2,7], Georg Stoecklin[8,9*] and Alessia Ruggieri[1*].

[1] Heidelberg University, Medical Faculty Heidelberg, Department of Infectious Diseases, Molecular Virology, Center for Integrative Infectious Disease Research (CIID), Germany, 69120 Heidelberg, Germany.

[2] Faculty of Health and Medical Sciences, School of Biosciences and Medicine, University of Surrey, Guildford, United Kingdom.

[3] Digital Health Center, Berlin Institute of Health (BIH) and Charité, 10178 Berlin, Germany.

[4] Medical Oncology, National Center for Tumor Diseases, Heidelberg University, 69120 Heidelberg, Germany.

[5] Leibniz-Forschungsinstitut für Molekulare Pharmakologie, 13125 Berlin, Germany.

[6] Freie Universität Berlin, Faculty of Biology, Chemistry, and Pharmacy, 14195 Berlin, Germany.

[7] The Pirbright Institute, Pirbright, United Kingdom.

[8] Division of Biochemistry, Mannheim Institute for Innate Immunoscience (MI3) and Mannheim Cancer Center (MCC), Medical Faculty Mannheim, Heidelberg University, 68167 Mannheim, Germany.

[9] Center for Molecular Biology of Heidelberg University (ZMBH), DKFZ-ZMBH Alliance, 69120 Heidelberg, Germany.

Correspondence:

*Alessia Ruggieri (Alessia.Ruggieri@med.uni-heidelberg.de, https://orcid.org/0000-0001-9981-3308)

*Georg Stoecklin (Georg.Stoecklin@medma.uni-heidelberg.de, https://orcid.org/0000-0001-9284-9834)

**Summary**

The integrated stress response (ISR) is a key cellular signaling pathway activated by environmental alterations that represses protein synthesis to restore homeostasis. To prevent sustained damage, the ISR is counteracted by the upregulation of Growth Arrest and DNA Damage inducible 34 (GADD34), a stress-induced regulatory subunit of protein phosphatase 1 that mediates translation reactivation and stress recovery. Here, we uncover a novel ISR regulatory step at the level of GADD34 mRNA post-transcriptional modification. We established that GADD34 mRNA 3' untranslated region contains an active AU-rich element recognized by proteins of the ZFP36 family, which promotes its rapid decay under normal conditions and stabilization for efficient expression of GADD34 protein in response to stress. We identify the tight temporal control of GADD34 mRNA turnover as a central element of the ISR molecular memory, which sets the threshold for cellular responsiveness and mediates adaptation to recurring and chronic stress conditions.

**Keywords**

Integrated stress response, GADD34, AU-rich element, mRNA decay, ZFP36, TTP, Brf1, molecular memory, stress recovery, chronic stress.

## Introduction

The integrated stress response (ISR) is a highly sensitive signaling network that allows cells to quickly react and adapt to a variety of potentially harmful perturbations, including cellular damage, environmental stress and viral infections. Signals are transduced by four different kinases, namely heme-regulated inhibitor (HRI), general control nonderepressible 2 (GCN2), protein kinase R (PKR) and PKR-like endoplasmic reticulum kinase (PERK), whose activation results in the direct phosphorylation of a common downstream substrate, the alpha subunit of the eukaryotic translation initiation factor 2 (eIF2$\alpha$) (Pakos-Zebrucka et al., 2016). This step reduces the availability of the active Met-tRNA$_i^{Met}$/eIF2/GTP ternary complex and leads to stalling of translation initiation followed by ribosome run-off and polysome disassembly (Hinnebusch, 2011). As a result, high local concentrations of released mRNAs and RNA-binding proteins trigger cytosolic phase separation and thereby drive the condensation of stress granules (SGs) (Riggs et al., 2020). In parallel, translational attenuation by increased levels of phosphorylated eIF2$\alpha$ (p-eIF2$\alpha$) promotes the expression of Growth Arrest and DNA Damage inducible 34 (GADD34), a stress-induced adaptor protein that in complex with protein phosphatase 1 (PP1) mediates the dephosphorylation of eIF2$\alpha$ (Brush et al., 2003; Ma and Hendershot, 2003; Novoa et al., 2001). This negative feedback loop antagonizes prolonged activation of the ISR, allowing resumption of translation and return to homeostasis (Novoa et al., 2003).

Under normal conditions, maintenance of eIF2$\alpha$ in its non-phosphorylated form is essential for continuous protein translation. This is primarily achieved by the constitutive repressor of eIF2$\alpha$ phosphorylation (CReP), an alternative adaptor protein that targets PP1 to eIF2$\alpha$ (Jousse et al., 2003). In the absence of stress, GADD34 mRNA is expressed at low levels and its translation is repressed by two non-overlapping upstream open frames (uORFs) within the 5' untranslated region (UTR). Under stress conditions, when the availability of active ternary complex is limiting, uORF translation ceases and ribosomal read-through allows translation of the GADD34 main ORF (Lee et al., 2009; Young et al., 2015). At the same time, two stress-responsive transcription factors, the activating transcription factor 4 (ATF4) and the C/EBP homologous protein (CHOP), are upregulated and induce expression of the *PPP1R15A* gene encoding GADD34 at the transcriptional level (Fawcett et al., 1999; Harding et al., 2000; Marciniak et al., 2004). Throughout this process, the GADD34 protein is short-lived as a result of proteasomal degradation, enabling tight temporal control of its levels (Brush and Shenolikar, 2008; Zhou et al., 2011; Zhou et al., 2013).

We have previously described a unique example of a highly dynamic stress response to hepatitis C virus (HCV) infection, characterized by alternating phases of SG assembly and disassembly, which coincide with phases of stalled and active translation, respectively (Ruggieri et al., 2012). By integrating quantitative experiments with mathematical modelling, we recently established the molecular network

generating this dynamic stress response and identified stochastic bursts of GADD34 expression and rapid GADD34 protein turnover as important determinants of this unique temporal control (Klein et al., 2022). Unexpectedly, we found that GADD34 mRNA levels remain elevated for a prolonged period after stress release, beyond the time when transcription is turned off. Thus, GADD34 mRNA acts as a molecular memory of previous ISR activation, facilitating subsequent bursts of GADD34 protein synthesis and faster changes in p-eIF2$\alpha$ levels when cells are exposed to prolonged or recurrent stress conditions (Klein et al., 2022). These findings raise the question whether active control of GADD34 mRNA stability might serve as an additional, post-transcriptional layer at which the ISR is regulated.

The balance between transcription and decay determines the abundance of every mRNA(Darnell, 1982). mRNA turnover is frequently regulated by *cis*-acting elements in the 3' UTR, which can enhance or repress the stability of mRNAs (Wilusz et al., 2001). Among them, AU-rich elements (AREs) represent a major class of mRNA destabilizing elements (Chen and Shyu, 1995) whose recognition by different RNA-binding proteins (RBPs) causes rapid mRNA degradation (Carballo et al., 1998; Chen et al., 2001; Stoecklin et al., 2002; Zhang et al., 1993), suppresses translation (Piecyk et al., 2000; Tiedje et al., 2012) or enhances transcript stability (Fan and Steitz, 1998). Rapid degradation of ARE-containing mRNAs is initiated through deadenylation by the CCR4/NOT complex(Sandler et al., 2011), followed by decay from the 3' end through the exosome (Chen et al., 2001; Mukherjee et al., 2002; Sandler et al., 2011) or from the 5' end by decapping and the exoribonuclease XRN-1 (Gao et al., 2001; Stoecklin et al., 2006).

The human tristetraprolin (TTP, also known as ZFP36) family comprises three closely related RBPs: TTP, Butyrate Response Factor 1 (Brf1, also known as ZFP36L1) and Brf2 (ZFP36L2), all of which bind to the ARE of their target mRNAs through two tandem CCCH-type zinc finger domains (TZDs) (Lai et al., 2000). The activity of TTP and Brf1 is regulated by inhibitory phosphorylation at several serine residues upon activation of the mitogen-activated protein kinase p38 (p38-MAPK)–MK2 pathway (Chrestensen et al., 2004; Johnson et al., 2002; Maitra et al., 2008; Stoecklin et al., 2004a). Brf1 is additionally phosphorylated at serine residue 92 by the phosphatidylinositol 3-kinase (PI3K)/Akt pathway (Benjamin et al., 2006; Schmidlin et al., 2004). Phosphorylation of TTP and Brf1 prevents ARE-mediated mRNA decay and enables efficient translation of target mRNAs (Benjamin et al., 2006; Schmidlin et al., 2004; Stoecklin et al., 2004a; Tiedje et al., 2012; Zhao et al., 2011).

Here, we investigated the post-transcriptional regulation of GADD34 mRNA stability and uncovered its role in regulating the ISR. We identified a functional ARE in the GADD34 3' UTR, which is recognized by TTP and Brf1, and promotes rapid GADD34 mRNA decay under normal conditions. Exposure to different types of stress simultaneously activates the p38-MAPK/MK2 and PI3K/Akt pathways, leading to downstream phosphorylation of TTP and Brf1 as well as to the rapid, transient stabilization of GADD34 mRNA. Our findings reveal that regulation of GADD34 mRNA stability controls the cellular sensitivity and reactivity to stress, and the kinetics of recovery from ISR activation.

**Results**

**Exposure to stress enhances GADD34 mRNA stability**

We hypothesized that in addition to regulation at the transcriptional and translational level, GADD34 mRNA degradation rates may provide additional control of the dynamic response to HCV infection (Klein et al., 2022). To examine this possibility, we first measured GADD34 mRNA turnover in cells under normal conditions by actinomycin D chase experiments and quantitative real-time PCR (qRT-PCR), using the stable GAPDH mRNA as a control. Intriguingly, we found GADD34 mRNA to be short-lived compared to GAPDH mRNA, with a half-life of approximately 1.2 hours ($t_{1/2}$, Figure 1A). Upon HCV infection and activation of PKR by viral double-stranded (ds) RNA replication intermediates, GADD34 mRNA was weakly stabilized ($t_{1/2}$ = 1.6 hours, Figure S1A), an effect that was stronger when the infection occurred in the presence IFN-$\alpha$ ($t_{1/2}$ = 2.4 hours, Figure 1B left panel). Interestingly, stabilization was more pronounced in cells transfected with synthetic dsRNA ($t_{1/2}$ > 10 hours, Figure 1B right panel), indicating that GADD34 mRNA turnover is not regulated by viral proteins. We next examined GADD34 mRNA turnover in response to potent chemical stress inducers that activate different eIF2$\alpha$-kinases. We chose sodium arsenite, which induces oxidative stress through the activation of HRI, and thapsigargin, an inducer of PERK-mediated ER stress (Taniuchi et al., 2016). Remarkably, acute treatment of cells with either stressor led to a strong inhibition of GADD34 mRNA degradation ($t_{1/2}$ > 10 hours, Figures S1B and S1C).

Unlike chronic HCV infection, chemical stressors trigger a single burst of SGs. For instance, high doses of thapsigargin induce the synchronized formation of SGs within 10 minutes, which disassemble approximately 2 to 4 hours after treatment, when GADD34 protein becomes detectable(Klein et al., 2022; Ruggieri et al., 2012). We took advantage of the ability of thapsigargin-treated cells to survive for more than 12 hours to obtain a time-resolved insight into GADD34 mRNA turnover over a longer period of stress (Figure 1C). Thapsigargin strongly inhibited GADD34 mRNA decay within the first three hours of treatment (1h Thap + 2h actinomycin D chase), resulting in a markedly stabilized mRNA (Thap 1h, $t_{1/2}$ > 10 hours, Figure 1C). Thereafter, GADD34 mRNA half-life gradually decreased over time, reaching at 12 hours a value in the range of that observed in IFN-$\alpha$ treated HCV-infected cells ($t_{1/2}$ = 2.4 hours). This value remained significantly higher than that measured under normal conditions (DMSO, $t_{1/2}$ = 1.3 hours, Figure 1C).

Altogether, these results demonstrate that GADD34 mRNA turnover is dynamically regulated in response to the activation of the ISR by different triggers, suggesting that GADD34 mRNA stabilization represents a conserved mechanism that contributes to the ISR negative feedback loop.

**GADD34 mRNA turnover involves a destabilizing AU-rich element in the 3' untranslated region**

Targeted control of mRNA degradation is frequently mediated by RBPs that recognize specific binding sites located in the 3' UTR of mRNAs (Garcia-Maurino et al., 2017). With 85 nucleotides, the 3' UTR of human GADD34 mRNA is particularly short and comprises 70 percent adenosine (A) and uridine (U) residues (Figure 1D). Further inspection of the GADD34 3' UTR sequence identified two canonical AUUUA

pentamers embedded in U-rich clusters typical for AREs, a major class of mRNA destabilizing elements (Chen and Shyu, 1995; Zubiaga et al., 1995). To examine whether GADD34 mRNA turnover is regulated via a functional ARE, we generated stable Huh7 cell lines expressing a rabbit β-globin reporter gene (Leppek et al., 2013) in which we inserted, between the stop codon and the β-globin 3' UTR, either the wild type 3' UTR sequence of GADD34 or a mutated sequence where both AUUUA pentamers were converted to AUGUA ($GADD34_{MUT}$) (Figure 1E). As positive control, we used a β-globin reporter gene harboring the ARE of tumor necrosis factor-α (TNF-α) known to strongly accelerate mRNA decay (Carballo et al., 1998; Leppek et al., 2013; Stoecklin et al., 2004a). Remarkably, insertion of the GADD34 3' UTR promoted the decay of the otherwise stable β-globin reporter mRNA (WT, $t_{1/2}$ = 12.3 hours) almost as efficiently (GADD34, $t_{1/2}$ = 2.9 hours) as the TNF-α ARE ($t_{1/2}$ = 2.5 hours) (Figure 1F). Mutation of the two AUUUA pentamers prevented rapid mRNA turnover ($GADD34_{MUT}$, $t_{1/2}$ = 8.3 hours), confirming the presence of an active ARE with destabilizing activity in the GADD34 3' UTR.

AREs interact with a range of RBPs and reduce the stability and translational activity of mRNAs (Fukao and Fujiwara, 2017). To investigate the impact of the 3' UTR on GADD34 mRNA translation efficiency, we analyzed the association of WT, GADD34 and $GADD34_{MUT}$ β-globin reporter mRNAs with polysomes by sucrose density gradient centrifugation, followed by fractionation, RNA isolation and qRT-PCR (Figure S1D). The distribution of the reporter mRNAs in the sub-polysomal and polysomal fractions showed that the GADDD34 3' UTR did not influence the association of the β-globin reporter mRNAs with polysomes, ruling out a direct effect on translation (Figure S1E).

To consolidate this result, we sought to explore the impact of deleting the ARE from the endogenous GADD34 locus, located in the third exon of the *PPP1R15A* gene (Figure S1F). We generated GADD34ΔARE single-cell clones using the CRISPR-Cas9 technology and nucleofection of two CRISPR RNAs (crRNAs) targeting the regions immediately upstream and downstream of the ARE. Three homozygous KO cell clones were selected by analysis of the *PPP1R15A* genomic sequence (Figure S1F). Additionally, control cell clones (Ctrl) were generated for comparison by nucleofection of non-targeting crRNAs. We analyzed GADD34 expression levels at steady state and upon treatment with thapsigargin. While deletion of the ARE did not alter basal GADD34 mRNA levels (Figure 1G), it resulted in a stronger increase of GADD34 mRNA levels, particularly at 6 hours post exposure to thapsigargin (Figure 1H). This result was supported by the slower decay of GADD34 mRNA measured during stress recovery, after treatment with thapsigargin for 3 hours (Figure 1I, 3h Thap: Ctrl $t_{1/2}$ = 1.7 hours, ΔARE $t_{1/2}$ >10 hours). Interestingly, though moderate, GADD34ΔARE cells showed a significant increase in basal GADD34 mRNA half-life (Figure 1I, DMSO: Ctrl $t_{1/2}$ = 0.9 hours, ΔARE $t_{1/2}$ = 1.2 hours). Additionally, polysome profile analysis confirmed that GADD34 mRNA associates with light polysomal fractions, consistent with its translation being attenuated by two upstream open reading frames (Lee et al., 2009), and was not affected by the absence of the ARE (Figure S1G). Altogether, these results suggest that GADD34 ARE does not affect the efficiency of translation but primarily regulates mRNAs stability in both unstressed and stressed cells, during the recovery period.

**GADD34 ARE is recognized by RNA-binding proteins of the ZFP36 family**

Next, we interrogated the GADD34 3' UTR for destabilizing RBP binding sites using RBPDB, a database that identifies RBP binding sites based on sequences retrieved from *in vitro* and *in vivo* RNA-binding experiments (Cook et al., 2011). The nonameric sequence CUAUUUAUU was highly scored as a potential binding site for TTP (ZFP36) (Figure 1D), a prediction confirmed by the AREsite2 database (Fallmann et al., 2016).

ZFP36 family proteins represent the most potent inducers of ARE-mRNA decay (Schott and Stoecklin, 2010) and comprise three members, TTP, Brf1 and Brf2, all of which contain a CCCH-type TZD with high affinity for AREs (Ciais et al., 2013). The TZF domains of ZFP36 proteins share 70 percent sequence identity, and there is evidence that TTP and Brf1 family members share some common target mRNAs (Tan and Elowitz, 2014) but also have preferences for specific ARE-mRNAs (Moore et al., 2018; Worthington et al., 2002). We therefore investigated both TTP and Brf1. In line with its function as an immediate early gene (Mahmoud et al., 2019; Tchen et al., 2004), the basal expression of TTP was low at steady state compared to Brf1 (Figure S2A), but transiently induced by stimulation with thapsigargin (Figure S2B).

First, we assessed the ability of the two ZFP36 family members to bind to endogenous GADD34 mRNA under normal conditions. To overcome problems of antibody specificity and availability, we transiently expressed myc-his-tagged human TTP and Brf1 (Figure S3A) at low levels to avoid the spontaneous formation of SGs (Kedersha et al., 2005; Stoecklin et al., 2004a). We also included the TTP murine orthologue (msTTP) and its previously characterized RNA-binding mutant, harboring a CCCH to SSCH mutations in both TZF domains ($msTTP_{m1,2}$) (Sandler et al., 2011). Myc-his-tagged GFP served as control for unspecific RNA binding. RNA-immunoprecipitation revealed that, in contrast to GAPDH mRNA, endogenous GADD34 mRNA was efficiently immunoprecipitated with TTP, msTTP and Brf1, but not $msTTP_{m1,2}$ (Figure 2A), confirming the importance of the TZF domain in the interaction of ZFP36 proteins with GADD34 mRNA.

Although predominantly located in 3' UTRs, AREs are also distributed in the intronic regions of some pre-mRNAs (Bakheet et al., 2018). To ensure that ZFP36 proteins specifically bind to the ARE located in the 3'UTR of GADD34 mRNA, we performed similar experiments using the β-globin reporter cell lines transiently expressing myc-his-tagged RBPs (Figure 2B). The reporter mRNA harboring the GADD34 3'UTR was strongly enriched following immunoprecipitation of TTP, Brf1 and msTTP, but not $msTTP_{m1,2}$ (Figure 2B). Despite being significantly reduced, the binding of the reporter mRNA harboring the $GADD34_{MUT}$ 3'UTR was not completely abrogated, suggesting that other sequences or secondary structures outside of the two AUUUA pentamers may contribute to the binding of ZFP36 proteins to GADD34 mRNA. Together, these results identified the ZFP36 members TTP and Brf1 as GADD34 ARE-interacting proteins.

**Ectopic expression of TTP and Brf1 destabilizes GADD34 mRNA**

Previous studies have suggested that TTP and Brf1 recruit the mRNA decay machinery to selectively degrade ARE-mRNAs (Lykke-Andersen and Wagner, 2005; Sandler et al., 2011). We therefore investigated the impact of ectopically expressed TTP and Brf1 on GADD34 mRNA turnover under stress conditions. Cells transiently expressing myc-his tagged ZFP36 proteins were treated with thapsigargin for different periods of time (Figure S3A). Phosphorylated eIF2$\alpha$ levels increased 1 hour after treatment in all cell lines, and decreased at 3 hours, mirroring the appearance of GADD34 protein (Figure 3A). At 6 hours post treatment, GADD34 mRNA and protein levels were markedly lower in cells expressing TTP, Brf1 or msTTP compared to those expressing GFP or msTTP$_{m1,2}$ (Figures 3A and 3B). At 3 hours post treatment, the reduction was only detectable at the protein level, possibly due to the detection of partially deadenylated and/or degraded transcripts by qRT-PCR.

To validate our results, we analyzed GADD34 mRNA decay over time in the different cell lines in the absence (DMSO) and presence of thapsigargin. In control cells expressing GFP or msTTP$_{m1,2}$, the decay kinetics of GADD34 mRNA was as previously observed in parental cells (Figure 1C), with a strong stabilization within 1 hour of treatment followed by a gradual return of decay by 6 hours post treatment (Figure 3C, same data arranged differently in Figure S3B). Interestingly, this dynamic was altered in cells expressing TTP, Brf1 or msTTP, in which GADD34 mRNA returned faster to rapid decay upon the initial stabilization by thapsigargin treatment, with the strongest difference observed at 3 hours after thapsigargin addition (Figure 3C). These results demonstrate that ZFP36 proteins accelerate the clearance of GADD34 mRNA during the recovery phase of the stress response and indicate that ZFP36 proteins are initially inactivated during the acute phase of the stress response.

**Acute and chronic stresses activate the p38-MAPK/MK2 and PI3K/Akt signaling pathways**

TTP and Brf1 activity is downregulated by their phosphorylation via the p38-mitogen-activated protein kinase (MAPK)/MK2 and PI3K/Akt signaling pathways (Schmidlin et al., 2004; Stoecklin et al., 2004a). We thus explored whether the stress response induced by acute treatment with thapsigargin or chronic HCV infection could represent a signal for MAPK activation using a commercially available phospho-MAPK array (Figure S4A). We detected a strong increase of Akt phosphorylation in response to both acute thapsigargin treatment and HCV chronic infection, whereas phosphorylation of p38$\alpha$ increased only after thapsigargin treatment. By using another set of antibodies and Western blot analyses, we confirmed that both pathways are activated by HCV infection (Figures 4A and 4B) and thapsigargin (Figures S4B and 4C).

To obtain insight into the dynamics of p38-MAPK/MK2 and PI3K/Akt pathway activation, we analyzed the phosphorylation levels of p38 and Akt at different time points after treatment with thapsigargin (Figure 4C). The levels of phosphorylated p38 (p-p38) and Akt (p-Akt) increased within the first hour of treatment, preceding the induction of GADD34 protein expression observed at 2 to 3 hours after treatment. During the stress recovery period, i.e. from 3 hours onwards, p-p38 and p-Akt levels started to decrease, concomitantly with the increase in GADD34 protein levels (Figures 4C and 4D).

To mimic the acute phase of an infection, pathway activation was also analyzed at 8, 16 and 24 hours post dsRNA transfection. While difficult to detect for p-Akt, p-p38 levels were increased at 8 hours and decreased over time (Figures S4D and S4E). A similar dynamics of pathway activation was also observed with sodium arsenite, within a shorter window of treatment that allowed cells to survive (Figures S4F and S4G). Taken together, these results show that the p38-MAPK/MK2 and PI3K/Akt signaling pathways are transiently activated during the ISR.

Next, we assessed whether p38-MAPK/MK2 and PI3K/Akt signaling influence GADD34 protein expression using pharmacological inhibition. SB203580 is a selective inhibitor of p38-MAPK activity, which also interferes with Akt activation (Lali et al., 2000). As previously described (Kumar et al., 1999), pre-treatment of cells with SB203580 inhibits p38-MAPK catalytic activity as measured by the absence of HSP27 phosphorylation, a downstream target of MK2 (Xu et al., 2006), whereas phosphorylation of p38 by upstream kinases is not affected (Figure S4H). While cells treated with SB203580 expressed significantly less GADD34 protein upon thapsigargin treatment (Figure S4I), this effect is most likely due to transcriptional inhibition of the *PPP1R15A* gene since both GADD34 pre-mRNA and mRNA levels were strongly reduced (Figures S4J and S4K). This observation is in line with previous reports showing that p38-MAPK is required for the phosphorylation the C/EBP homologous protein (CHOP) (Wang and Ron, 1996), a transcription factor involved in stress-dependent GADD34 induction (Fawcett et al., 1999; Harding et al., 2000).

We next perturbed the Akt signaling pathway using MK-2206, a pan Akt inhibitor (Zhao et al., 2014) (Figure S4H). Treatment of cells with MK-2206 prior to thapsigargin also attenuated GADD34 protein induction (Figures S4H and S4I). Importantly, and in contrast to SB203580, MK-2206 did not affect *PPP1R15A* transcription (Figure S4J).

Taken together, these results show that the activation of both the p38-MAPK/MK2 and PI3K/Akt signaling pathways participates in the induction of GADD34 during the ISR, triggering a negative feedback loop that promotes cellular recovery from stress.

**Activation of the ISR leads to transient hyper-phosphorylation of ZFP36 proteins**

Both TTP and Brf1 are multiply phosphorylated in cells (Johnson et al., 2002; Taylor et al., 1995; Zhu et al., 2001). We therefore assessed changes in the global phosphorylation levels of TTP and Brf1 over time in thapsigargin-treated cells. To this end, and to overcome the lack of specific antibodies, extracts of myc-his tagged TTP and Brf1 expressing cells were separated by Phos-tag polyacrylamide gel electrophoresis (Figures 4E and 4F). The phosphorylation pattern was compared to that of the non-phosphorylated forms, obtained by treatment of the extracts with lambda protein phosphatase (λPPase). As previously reported, the presence of multiple slower-migrating bands indicated that TTP and Brf1 are extensively phosphorylated under normal conditions (0 h). Stimulation with thapsigargin resulted in a visible shift towards a hyper-phosphorylated form of TTP and Brf1 within the first hour of treatment, whose level decreased continuously thereafter, reaching almost basal levels 12 hours after treatment (12 h). The

dynamic regulation of ZFP36 protein phosphorylation correlated with the activation kinetics of the PI3K/Akt and p38-MAPK/MK2 signaling pathways, and coincided with the decreased decay activity measured during the acute phase of the stress response. During the stress recovery period, dephosphorylation of ZFP36 proteins went along with the decreasing MAPK activity and decreasing GADD34 expression levels. Altogether, these results suggest that ZFP36 proteins are induced yet inactivated by hyperphosphorylation during the initial phase of the ISR, thereby enabling efficient GADD34 expression and entry into the stress recovery phase. Later in the recovery phase, gradual dephosphorylation of TTP and Brf1 promotes the degradation of GADD34 mRNA.

**TTP and Brf1 transiently localizes to SGs upon acute ER stress**

Depending on the type of environmental stress and their phosphorylation state, TTP and Brf1 localize to SGs, e.g. in response to energy deprivation or heat shock, but not to sodium arsenite-induced oxidative stress, which leads to TTP and Brf1 hyper-phosphorylation (Murata et al., 2005; Stoecklin et al., 2004a). We next determined their subcellular localization of the myc-his tagged RBPs in cells treated for 1 hour with thapsigargin. In unstressed cells, TTP mainly localized in the cytosol (Figure S4L). Upon thapsigargin treatment, a small fraction of both ZFP36 proteins localized to discrete SGs together with eIF3b, a canonical SG-resident protein (Aulas et al., 2017). Brf1 showed both nucleoplasmic and cytoplasmic localization in unstressed cells, and relocalized to the cytosol and cytosolic SGs in thapsigargin treated cells (Figure S4L). Based on previous findings (Stoecklin et al., 2004a) and considering that only a fraction of TTP and Brf1 is inactivated by hyper-phosphorylation upon treatment with thapsigargin (Figures 4E and 4F), we hypothesize that SGs might contribute in the sequestration of the remaining TTP and Brf1.

**ZFP36 proteins attenuate GADD34 expression during the ISR**

To further evaluate the role of TTP and Brf1 in the post-transcriptional regulation of GADD34, we generated TTP and Brf1 KO cell clones using a CRISPR/Cas9 two-guide strategy, with crRNAs targeting the regions immediately upstream and downstream of the *ZFP36 and ZFP36L1* TZDs (Figure S5A). The deletion of the genomic DNA sequences between the two targeted sites was confirmed in the independent cell clones by PCR and sequencing. Control cell clones (Ctrl) were generated for comparison using a non-targeting crRNA. While GADD34 steady state mRNA levels appeared slightly elevated in the TTP and Brf1 KO cell clones, the differences were not statistically significant (Figure 5A). In contrast to the results previously obtained with the GADD34 ΔARE cell clones, GADD34 mRNA turnover was not altered in unstressed TTP and Brf1 KO cell clones (Figures 5B and 5C). Interestingly, under stress conditions induced by thapsigargin for 3 hours, GADD34 mRNA was slightly stabilized in TTP KO compared to Ctrl and Brf1 KO cell clones (Figures 5D and 5E). This result was also supported by a moderate increase in GADD34 protein levels at 6 hours post thapsigargin treatment (Figure S5B).

Since the effects in the single KO clones were moderate, we explored the possibility of a functional redundancy by creating double KO (DKO) cell clones, in which TTP was knocked out in a Brf1 KO

background (Figure S5C). Under normal conditions, albeit not statistically significant, the loss of both TTP and Brf1 moderately increased GADD34 mRNA levels (Figure 5F). Interestingly, GADD34 mRNA was stabilized both in unstressed and stressed DKO cells (Figures 5G and 5H). The effect was even more pronounced at the protein level, with a 1.8-fold increase in the basal expression of GADD34 protein in the DKO cell clones (Figures 5I and 5J). This increase was not attributable to enhanced translation initiation, as reflected by polysome profile analyses (Figure S5D), or pre-activation of the ISR, as indicated by unchanged p-eIF2$\alpha$ levels (Figures 5I and 5J). Upon treatment with thapsigargin for longer periods of time, GADD34 protein levels increased more strongly in DKO cell clones than in Ctrl clones (Figures 5K and 5L), reflecting the results observed in TTP KO cells. In light of these results, we hypothesized that TTP and Brf1 have redundant roles in the regulation of GADD34 mRNA turnover under normal conditions. In response to stress and during the recovery phase, TTP appears to be the dominant regulator of GADD34 mRNA stability, consistent with the more dynamic expression pattern of TTP.

**ZFP36 proteins regulate sensitivity and responsiveness to stress**

We previously found that the sustained presence of GADD34 mRNA confers a transient adaptation to stress and a different responsiveness to stress during the stress recovery phase (Klein et al., 2022). Directly after stress release, cells enter a refractory phase, in which the remaining GADD34 proteins dephosphorylate eIF2$\alpha$, effectively repressing the cellular stress response. The full responsiveness to stress is only regained after 20 hours, at which time GADD34 mRNA returns to its basal level (Klein et al., 2022). We therefore hypothesized that increased expression of GADD34 in DKO cells could reduce the responsiveness to stress and confer a higher level of stress adaptation. To test this hypothesis, we first assessed the stress responsiveness of DKO cell clones by measuring their ability to form SGs in response to increasing doses of sodium arsenite (Figures 6A and S6A). As predicted, the DKO clones showed reduced SG formation after challenge with intermediate doses of sodium arsenite (100 to 250 µM), with the most striking difference at 100 µM, where approximately 50% of the Ctrl cells formed SGs compared to only 20% of the DKO cells. This result confirms that higher basal expression of GADD34 in DKO cells reduces their sensitivity to environmental stress, raising the threshold at which the ISR is triggered.

We next asked how prolonged expression of GADD34 during recovery from a first stress would influence the responsiveness of DKO clones to a second stress stimulus. To this end, Ctrl and DKO cell clones were pre-treated with thapsigargin for 6 or 12 hours, followed by an acute pulse of high dose sodium arsenite (Figure 6B). In agreement with our previous work (Klein et al., 2022), pre-exposure of Ctrl clones to a 6-hour thapsigargin treatment strongly attenuated the phosphorylation of eIF2$\alpha$ (Figures 6B and 6C). This was associated with the formation of SGs in about 50 % of the cells (Figures 6D and S6B). In DKO cell clones, the pre-existing levels of GADD34 protein led to more pronounced dephosphorylation of eIF2$\alpha$, with only 20 % of cells forming SGs. At 12 hours, Ctrl cell clones had recovered almost entirely and 80 % of cells were able to form SGs, while DKO cell clones were still unable to mount an efficient SG response, with only about 50 % SG-positive cells. Taken together, these results indicate that post-transcriptional

control of GADD34 expression by ZFP36 proteins is critical for controlling responsiveness and cellular adaptation to stress at the onset of the ISR and during the recovery phase.

**Chronic exposure to low-dose stress increases GADD34 levels and impairs SG formation**

We recently described that continuous stress of moderate intensity caused by chronic HCV infection promotes long-term cell adaptation to stress (Klein et al., 2022). To determine whether the post-transcriptional control of GADD34 expression is also important during such conditions of prolonged stress, we compared DKO cells to Ctrl cells exposed to mild chronic stress (CS). To this end, Ctrl cells were maintained for five days in medium containing low dose sodium arsenite (2.5 µM), at which cells do not form SGs (Figure S6C). We then evaluated their responsiveness to an acute stress pulse by measuring p-eIF2$\alpha$ and GADD34 protein levels, and assessing their ability to form SGs. Chronically stressed cells were akin to the phenotype observed in DKO cells, with no detectable increase in p-eIF2$\alpha$ levels and higher steady state levels of GADD34 (Figures S6D and S6E). When subjected to an acute stress pulse with 50 µM sodium arsenite, chronically stressed cells behaved as DKO cells and expressed significantly lower levels of p-eIF2$\alpha$ than non-chronically stressed cells (Figure 6E and 6F). This reduced stress sensitivity was also reflected at the SG levels, as only about 25 % of chronically stressed cells were able to form SGs (Figures 6G and S6F). Altogether, these results suggest that loss of TTP and Brf1 function causes cells to enter a state that resembles chronic stress, with reduced responsiveness to acute stressors due to elevated expression of GADD34.

**Discussion**

Previous studies have suggested that GADD34 mRNA is intrinsically unstable (Rutkowski et al., 2006) and can be stabilized upon exposure to genotoxic stress (Jackman et al., 1994). However, the mechanism controlling GADD34 mRNA stability remained elusive. In this work, we unveiled a novel component of ISR regulation at the level of the GADD34 negative feedback loop and identified changes in the ARE-mediated decay of GADD34 mRNA as a key mechanism that links the cellular experience of previous stress to its responsiveness towards novel stress exposure (Figure 7). Under basal conditions, recognition of the 3' UTR ARE by members of the ZFP36 family results in the rapid decay of GADD34 mRNA, thereby attenuating GADD34 protein synthesis while making sure its mRNA is continually produced. With an estimated half-life below 1.5 hours, GADD34 mRNA classifies among the five percent of fast-decaying cellular mRNAs (Yang et al., 2003).

When cells encounter stress conditions, the regulatory circuit switches: GADD34 mRNA is markedly stabilized within the first few hours of stress, due to phosphorylation-induced inactivation of the ZFP36 proteins by the stress-activated p38-MAPK/MK2 and PI3K/Akt signaling pathways. This promotes GADD34 protein production, which triggers transition to the stress recovery phase. The mechanism by which TTP and Brf1 are inactivated upon phosphorylation has been characterized previously: it involves binding of 14-3-3 adaptor proteins to phosphorylated TTP or Brf1 (Schmidlin et al., 2004; Stoecklin et al.,

2004a), which leads to reduced association with the deadenylase machinery that triggers mRNA decay (Clement et al., 2011), and may further cause reduced affinity of ZFP36 proteins for ARE-containing target mRNAs (Tiedje et al., 2012).

Stress-induced stabilization of GADD34 mRNA is transient and gradually decreases upon dephosphorylation and reactivation of ZFP36 proteins as cells recover from stress. Our results and provide mechanistic insight into how GADD34 mRNA levels are regulated. The persistence of GADD34 mRNA above basal levels after stress recovery serves as a molecular memory of the previously activated ISR, and allows for rapid translation of GADD34 in response to an increase in p-eIF2$\alpha$ levels when cells encounter subsequent or continued stress. This molecular memory imposes a refractory phase and reduces responsiveness to stress by elevating the threshold at which the next ISR is triggered, thereby promoting cellular adaptation to acute and chronic stress of moderate intensity (Figure 7).

The multilayer regulation of the GADD34 negative feedback loop underscores how important it is for cells to maintain low levels of GADD34 mRNA under basal conditions. In line with this notion, deletion of the ARE at the endogenous PPP15R1A locus led to a moderate, albeit significant, stabilization of GADD34 mRNA. Notably, this effect was more pronounced under stress conditions. While a comparable phenotype has been previously reported upon deletion of the ARE in the TNF-$\alpha$ gene in mice (Kontoyiannis et al., 1999), other mechanisms may contribute to the rapid decay of GADD34 mRNA. For example, as reported for the yeast CPA1 mRNA, ribosome stalling at a uORF termination codon may activate nonsense-mediated mRNA decay (Gaba et al., 2005). Given that GADD34 translation in under control of two uORFs (Lee et al., 2009; Young et al., 2015), such a mechanism could potentiate the effect of ARE-mediated mRNA decay on GADD34 mRNA turnover. Other factors to consider are members of the Hu (also known as ELAV) family such as HuR (also known as ELAVL1), which have antagonistic functions to ZFP36 proteins and frequently stabilize ARE-containing mRNAs. Although HuR predominantly binds U- and CU-rich sequences, it recognizes over 80 % of the TTP binding sites (Mukherjee et al., 2014) and could therefore contribute to the stabilization of GADD34 mRNA under stress conditions. Depending on the cell type, differences in TTP, Brf1 and Hu expression levels may also play a role in determining the extent to which mRNA turnover controls GADD34 expression before, during and after the ISR.

Two of our observations suggest that ZFP36 family members are not simply redundant as temporal differences in their expression help to orchestrate the dynamics of GADD34 expression. First, their expression profile differs, with basal Brf1 mRNA levels being higher than those of TTP, while TTP mRNA expression levels exceed those of Brf1 in response to stress. Secondly, the results obtained with the single KO and DKO cell clones indicate that Brf1 activity is predominant under basal conditions, whereas TTP activity takes over in response to stress. Hence, it appears that the impact of ZFP36 family members follows the dynamics of their expression, and may render posttranscriptional control of GADD34 mRNA stability sensitive to different signaling pathways such as p38-MAPK (TTP and Brf1) and Akt (Brf1) (Maitra et al., 2008; Schmidlin et al., 2004; Stoecklin et al., 2004a). Whether the third member of the ZFP36 family, Brf2, would also contribute to this regulatory circuit remains to be investigated.

An important outcome of our study is that alterations in the post-transcriptional regulation of GADD34 mRNA and, consequently, GADD34 expression levels, critically affect cellular responsiveness to stress, the course of stress recovery and the duration of an ensuing ISR. Defective ARE-mediated mRNA decay in TTP and Brf1 DKO cells led to elevated basal expression of GADD34, which in turn reduced the responsiveness to stress. Following stress exposure, these cells required a longer period to regain full responsiveness. While a lower stress sensitivity may seem favorable at first sight, elevated GADD34 levels seem to come with a trade-off since the protein was found to affect other cellular functions. Increased GADD34 levels reportedly promote autophagy by suppressing mTOR signaling (Gambardella et al., 2020; Holczer et al., 2016; Ito et al., 2015). In addition, both pro- and anti-apoptotic functions have been assigned to GADD34, depending on its expression level (Hollander et al., 1997; Lee et al., 2018). In the future, it will be interesting to investigate the effect of elevated or prolonged GADD34 expression on cell survival and cellular homeostasis more generally. By exploring the memory function of GADD34 mRNA in recording cellular stress experience, and demonstrating the impact of GADD34 mRNA stability on memory timing, our study uncovers an unexpected link between the regulation of mRNA turnover and the intricate translational control system that governs the ISR. As a central node in the regulatory pathway controlling cellular adaptation to stress, GADD34 expression is a hallmark of cells constantly exposed to chronic stress.

**Acknowledgements**

We thank all members of the Ruggieri and Stoecklin laboratories for helpful discussions. We also thank the Infectious Diseases Imaging Platform (IDIP) at the CIID (Heidelberg University). We are grateful to Christine Clayton at the Center for Molecular Biology of Heidelberg University (ZMBH) for providing access to the equipment required for polysome profile analysis. This work was supported by the Deutsche Forschungsgemeinschaft (DFG, German Research Foundation) [project numbers 240245660 SFB1129 TP13 to A.R., 278001972 TRR186 A14 to A.R. and G.S., 278001972 TRR186 A08 to V.H., 439669440 TRR319 RMaP TP A05 to A.R. and 439669440 TRR319 RMaP TP A04 to G.S.]; by the Biotechnology and Biological Sciences Research Council research grants [grant numbers BB/S006931/1 and BB/P068018/1 to N.L.].

**Author contributions**

A.R. and G.S conceptualized the study. V.M., A.M., K.K., J.W. and L.E. performed and analyzed experiments. S.K. made a preliminary estimation of GADD34 mRNA stability using mathematical modelling. A.R., G.S., N.L. and V.M. drafted and edited the manuscript. V.H. critically revised the manuscript. All authors approved the final manuscript.

**Declaration of interests**

The authors declare that they have no competing interests.

**Lead Contact**

Further information and requests for resources and reagents should be directed to and will be fulfilled by the Lead Contact, Alessia Ruggieri (Alessia.Ruggieri@med.uni-heidelberg.de).

**Materials Availability**

All unique/stable reagents generated in this study are available from the Lead Contact with a completed Materials Transfer Agreement.

## METHODS

**Cell culture and culture conditions**

Huh7 cells, HEK293T cells and Huh7 GADD34ΔARE, Huh7 TTP knockout (KO), Huh7 Brf1 KO and Brf1-TTP double knockout (DKO) cell clones were cultivated in complete Dulbecco's modified Eagle medium (DMEM) supplemented with 10 % foetal calf serum (Capricorn), 2 mM L-glutamine, non-essential amino acids, 100 U/ml penicillin and 100 µg/ml streptomycin (all from Gibco). Huh7 cells stably expressing β-globin reporter constructs were generated by lentiviral transduction and subsequent selection in the presence of 5 µg/ml blasticidin (Blr).

**Generation of Huh7 knockout (KO) cell clones**

A two-crRNA strategy was used for the deletion and/or knockout of genomic sequences of interest. For the deletion of the ARE sequence from the endogenous PPP1R15A locus, two self-designed crRNAs flanking the ARE sequence were purchased from Integrated DNA technologies (target-specific sequence is shown in bold): sequence 1 (5' – / AltR1 / GAG GCG UGG CUG AGA CCA ACG UUU UAG AGC UAU GCU / AltR2 / – 3') and sequence 2 (5'– / AltR1 / UAU UUA UUU UUU CUA AGU GGU UUU AGA GCU AUG CU / AltR2 / – 3').

For the knockout of ZFP36 (TTP) and ZFP36L1 (Brf1) genes, two pre-designed crRNAs per target gene were purchased from Integrated DNA technologies (target-specific sequence is shown in bold): Hs.Cas9.ZFP36.1.AA (5' – / AltR1 / CCG UGC CAU CCG ACC AUG GAG UUU UAG AGC UAU GCU / AltR2 / – 3') and Hs.Cas9.ZFP36.1.AC (5' – / AltR1 / CCA CAA CCC UAG CGA AGA CCG UUU UAG AGC UAU GCU / AltR2 / – 3'), Hs.Cas9.ZFP36L1.1.AB (5' – / AltR1 / GGG UGA CUG AGU GCC UCC GAG UUU UAG AGC UAU GCU / AltR2 / – 3') and Hs.Cas9.ZFP36L1.1.AR (5' – / AltR1 / UGC CGC ACC UUC CAC ACC AUG UUU UAG AGC UAU GCU / AltR2 / – 3'). A negative control crRNA (Integrated DNA technologies) was used to generate control cell lines. Individual crRNAs and tracrRNA (Integrated DNA technologies) were resuspended in 1 x TE buffer (10 mM Tris, 0.1 mM EDTA, pH 7.5) to a final concentration of 200 µM and hybridized at equimolar amounts by heating to 95 °C for 5 min and slow stepwise cooling to room temperature. Pre-assembled crRNA/Cas9 ribonucleoprotein complexes (RNPs)

were obtained by gently mixing 1.2 µl of hybridized RNAs with 17 µg of recombinant Cas9 protein (Integrated DNA technologies) and 2.1 µl of PBS, followed by 20 min incubation at room temperature.

Huh7 cells (2 x $10^6$) were washed with PBS, resuspended in 91 µl supplemented Solution T (Lonza) and mixed with 2.5 µl of each pre-assembled RNP and 4 µl electroporation enhancer (Integrated DNA technologies). Nucleofection was performed using an Amaxa 2b nucleofector (Lonza) and pre-set program T-22. Nucleofected cells were incubated for 48 h prior to clonal amplification and screening for homozygous clones using target-specific PCR (GoTaq Hot Start, Promega) on genomic DNA using the following primers: TTP-KO-For: 5' – ACC TCC AAC TCT GGG TTC CT – 3'; TTP-KO-Rev: 5' – GAG AAG GCA GAG GGT GAC AG – 3'; Brf1-KO-For: 5' – GTG GTA GCT TTG GGG ACA GA – 3'; Brf1-KO-Rev: 5' – GTC ATC GGC GCT CAG AAT AG – 3'; ARE-seq-long-For 5' – ACC TTG CCT TCC TCC TCT GTC CCT – 3'; ARE-seq-long-Rev: 5' – GCT ATT CTC TTC CCA GCT CCC TCA -3'.

For Huh7 GADD34ΔARE cell clones, the resulting PCR product was purified and directly send for sequencing. For TTP and BRF1 KO and DKO cell clones, PCR product pools were further subcloned into a TOPO TA cloning vector (Thermo Fisher Scientific) according to manufacturer's recommendation and transformed into DH5α competent bacteria. Eight to ten colonies were selected and amplified for the extraction of plasmid DNA, which was then send for sequencing to ensure that all potential allelic sequence variants were covered.

**Plasmids**

pcDNA3-TTP-myc-his (msTTP) encoding tagged mouse TTP and pcDNA3-TTP-m1,2-myc-his ($msTTP_{1,2}$) encoding its RNA-binding mutant have been described elsewhere(Johnson et al., 2000; Stoecklin et al., 2004b).

*ZFP36* and *ZFP36L1* open reading frames, encoding human TTP and Brf1, respectively, were amplified from the ORFeome cDNA clone library (Invitrogen, Life Technologies) by Phusion PCR (Thermo Fisher Scientific) using the following primers bearing unique ClaI and XbaI restriction sites: ClaI-huTTP-For: 5' – ATA ACT ATC GAT ATG GAT CTG ACT GCC ATC TAC GAG – 3', XbaI-huTTP-Rev: 5' – ATT ACC TCT AGA CTC AGA AAC AGA GAT GCG ATT GAA – 3', ClaI-huBrf1-For: 5' – ATA TTT ATC GAT ATG ACC ACC ACC CTC GTG TCT GCC – 3', XbaI-huBrf1-Rev: 5' – GGC GAC TCT AGA GTC ATC TGA GAT GGA AAG TCT GCT – 3'. PCR products were digested with ClaI and XbaI (New England Biolabs) and inserted into pcDNA3-TTP-myc-his vector backbone digested with the same restriction enzymes.

For transient expression, sequences of all myc-his tagged RBPs were digested using ClaI and PmeI restrictions enzymes (New England Biolabs), blunted using DNA polymerase I large Klenow fragment (New England Biolabs) and inserted into a PmeI-linearized pWPI Puro lentiviral vector carrying a puromycin resistance gene.

pcDNA3-7B β-globin reporter (WT) and pcDNA3-7B TNFα ARE containing the ARE of mouse TNF-α (msTNFα-ARE) were described before(Ozgur et al., 2010; Stoecklin et al., 2003). Beta-globin reporter constructs expressing GADD34 3'UTR (pcDNA3-7B-β-globin reporter GADD34 human 3'UTR) or GADD34

3'UTR with mutated ARE pentamer motives (pcDNA3-7B-β-globin reporter GADD34 human mutated 3'UTR) were generated by insertion of the corresponding sequences upstream of beta-globin 3' UTR sequence using hybridized oligonucleotides with overhangs (shown in bold) compatible to those produced by BglII digest. The following oligonucleotides were used: GADD34-3'UTR-For: 5' – **GAT C**TG ACC AAC TGG TTT GCC TAT AAT TTA TTA ACT ATT TAT TTT TTC TAA GTG TGG GTT TAT ATA AGG A – 3'; GADD34-3'UTR-Rev: 5' – GAT CTC CTT ATA TAA ACC CAC ACT TAG AAA AAA TAA ATA GTT AAT AAA TTA TAG GCA AAC CAG TTG GTC **A** – 3'; GADD34-3'UTR-mut-For: 5' – **GAT C**TG ACC AAC TGG TTT GCC TAT AAT GTA TTA ACT ATG TAT TTT TTC TAA GTG TGG GTT TAT ATA AGG A – 3'; GADD34-3'UTR-mut-Rev: 5' – GAT CTC CTT ATA TAA ACC CAC ACT TAG AAA AAA TAC ATA GTT AAT ACA TTA TAG GCA AAC CAG TTG GTC **A** – 3'. Equimolar amounts of complementary oligonucleotides were phosphorylated by incubation with T4 polynucleotide kinase in T4 ligation buffer (New England Biolabs) for 30 min at 37°C. Phosphorylated oligonucleotides were hybridized by heating the reaction to 95 °C for 5 min followed by slow stepwise cooling to room temperature. Hybridized oligonucleotides were then inserted into pcDNA3-7B digested with BglII. All β-globin reporter sequences were shuffled into a lentiviral vector for lentiviral transduction and selection of stable cell lines. To this end, pcDNA3-7B constructs were digested with HindIII and XbaI. The resulting fragments were blunted using DNA polymerase I large Klenow fragment (New England Biolabs) and inserted into a PmeI-linearized pWPI Blr lentiviral vector (Steinmann and Brohm, 2008) carrying a blasticidin resistance gene (pWPI GADD34 3'UTR Blr and pWPI GADD34 3'UTR mut Blr).

**Hepatitis C virus infection**

Huh7 cells were infected with full-length, replication competent hepatitis C virus (HCV) at an MOI of 5 for 24 h or with trans-complemented HCV particles ($HCV_{TCP}$) at an MOI of 10 for 48 h prior to the addition of 100 U/ml IFN-$\alpha$ for 24 h to induce an antiviral stress response as previously described(Ruggieri et al., 2012).

**Transfection with double-stranded (ds) RNA**

Synthesis and purification of 200-bp dsRNA was described previously (Klein et al., 2022). In brief, a 200-bp region from the ampicillin resistance gene was used as template for *in vitro* synthesis of plus and minus strand transcripts and hybridized. For the analysis of RNA turnover, 1.7 x $10^5$ Huh7 cells were seeded in a 6-well plate and transfected with 1 µg purified dsRNA mixed with Lipofectamin 2000 transfection reagent (Thermo Fisher Scientific) in a 1:3 ratio. For the protein analyses, 2.5 x $10^5$ cells were seeded in 6-cm dishes and transfected with 1.5 µg dsRNA accordingly. Transfected cells were incubated for 8, 16 or 24 h until harvest.

**Production of lentiviruses and cell transduction**

HEK293T cells (5 x $10^6$ in a 10-cm cell culture dish) were seeded on the day prior to transfection. Cells were transfected with 6.42 µg target gene-encoding pWPI plasmid, 6.42 µg pCMV Δ8.91 and 2.16 µg pMD2.G (kind gift from Didier Trono) (Zufferey et al., 1997), using polyethylenimine (PEI) solution (pH 7.2).

In brief, DNA was diluted with OptiMEM (Gibco) and mixed with PEI solution in a 1:3 (PEI:DNA) ratio. Samples were vortexed vigorously prior to incubation at room temperature for 20 min. Transfection mix was added dropwise to the cells and transfected cells were incubated for 48 h, replenishing media at 6 h post-transfection. Lentivirus-containing supernatant was filtered through 0.45 µm pore size filters and used to transduce target Huh7 cells. For the generation of stable cell lines, the corresponding antibiotic selection was added for 36 h after transduction and prior to cell amplification. For transient transductions, Huh7 were directly seeded into diluted lentiviral supernatant (diluted 1:10 in complete DMEM) at the following densities: 8 x $10^4$ cells per well in 12-well plates for the preparation of RNA; 2.5 x $10^5$ cells in 6-cm dishes for protein analysis. Medium was replenished after 24 h and cells harvested between 36 and 40 h.

**Chemical treatments**

Huh7 cells were seeded one day prior to treatment (5 x $10^4$ cells per well in 12-well plates for RNA extraction; 3 x $10^5$ cells in 6-cm dishes for protein analyses). Thapsigargin (Biotrend) was dissolved in DMSO and used at a concentration of 2 µM for up to 12 h. Sodium arsenite (Sigma Aldrich) was resuspended in $H_2O$ and used at a concentration of 500 µM for 45 min for the induction of acute stress response. For chronic arsenite exposure, cells (1 x $10^5$ in 6-well plates) were cultivated in the presence of 2.5 µM arsenite for 5 days. Cells were split on day 2 to avoid overgrowth and subjected on day 5 to a second stress pulse of 50 µM arsenite for 45 min to induce acute stress before harvest.

The Akt signaling pathway was inhibited using 10 µM MK-2206,2HCl (Selleckchem, dissolved in DMSO). The p38-MAPK signaling pathway was inhibited using 50 µM SB203580 (Sigma Aldrich, dissolved in DMSO). After pre-treatment with either inhibitor for 1 h, cells were co-treated with 2 µM thapsigargin for 3 h to induce GADD34 expression.

**Measurements of mRNA turnover**

Huh7 cells (5 x $10^4$ cells per well in 12-well) were treated with 5 µg/ml of actinomycin D (Sigma-Aldrich, dissolved in DMSO). Samples were harvested at the indicated times for total RNA extraction using the NucleoSpin RNA kit (Macherey Nagel) following the manufacturer's protocol, and further analyzed by qPCR. For a given target, the quantified expression of treated samples was normalized to the expression of an untreated control sample (T0) and expressed as a percentage to depict mRNA decay rate over time. The resulting decay curves were obtained by using non-linear regression using GraphPad Prism software to estimate the mRNA half-life ($t_{1/2}$). For half-lives exceeding 10 h or which could not be determined, values are indicated as "n.d. (> 10 h)".

**RNA immunoprecipitation**

Huh7 cells (8 x $10^5$ in 10-cm dishes) were seeded in the presence of filtered lentivirus supernatant diluted 1:3 in cell culture medium. After 24 h. medium was replenished. Between 36 and 40 h post transduction with lentiviruses expressing myc-his tagged proteins, Huh7 cells were washed twice with ice-cold PBS and

lysed by scraping cells on ice with 500 µl IP lysis buffer (50 mM Tris HCl pH 8.0, 150 mM NaCl, 1 mM $MgCl_2$, 1 % NP40, 2 % glycerol, 1 mM DTT, 1 mM $Na_3VO_4$, 50 mM NaF, supplemented with cOmplete mini protease inhibitor cocktail (Roche)). Two plates per condition were pooled into a fresh reaction tube. Lysates were incubated for 10 min on ice and subsequently centrifuged at 20,800 x g for 10 min at 4 °C. Supernatants were transferred into DNA LoBind tubes (Eppendorf) and two aliquots of 40 µl each were kept for later RNA and protein input analyses. Binding conditions were optimised by adding NaCl and imidazole to the lysates to achieve a final concentration of 250 mM NaCl, 10 mM imidazole. Ni-NTA agarose beads (Qiagen) were pre-washed twice with 500 µl IP lysis buffer and added to samples (50 µl/sample). After tumbling at 4 °C for 2 h, beads were washed 6 times by the addition of 1 ml IP wash buffer (50 mM Tris HCl pH 8.0, 250 mM NaCl, 1 mM $MgCl_2$, 1 % NP40, 2 % glycerol, 1 mM DTT, 1 mM $Na_3VO_4$, 50 mM NaF, 10mM imidazole, supplemented with cOmplete mini protease inhibitor cocktail (Roche)) and centrifugation at 2,650 x g for 3 min at 4 °C. After the last wash, samples were split, with one half used for protein elution and the other half for RNA extraction. For protein elution, beads were centrifuged once at 5,000 x g and resuspended in 30 µl IP elution buffer (50 mM Tris HCl pH 8.0, 500 mM NaCl, 1 mM $MgCl_2$, 1 % NP40, 2 % glycerol, 1 mM DTT, 1 mM $Na_3VO_4$, 50 mM NaF, 500 mM imidazole, supplemented with cOmplete mini protease inhibitor cocktail (Roche)). After 2 min incubation on ice, samples were centrifuged and supernatants transferred into fresh tubes. The elution procedure was repeated once and both eluates were pooled and stored at -70 °C until further analysis. Prior to RNA extraction, 360 µl of IP lysis buffer were added to RNA input samples to achieve equal sample volumes. 400 µl RNA extraction buffer (10 mM Tris HCl pH 7.5, 350 mM NaCl, 10 mM EDTA, 1 % SDS, 42 % urea) was added to lysates and each sample was spiked with 3 x $10^8$ copies of *firefly* luciferase *in vitro* transcripts to allow for later normalization of the values to RNA loss during purification. After the addition of 400 µl phenol/chloroform/isoamyl alcohol (25:24:1, v/v, Applichem) samples were vigorously vortexed prior to centrifugation at 20,800 x g for 15 min at room temperature. The aqueous upper phase was carefully recovered and transferred to fresh tubes. RNA was precipitated by addition of 800 µl isopropanol containing 0.2 % GlycoBlue (Invitrogen) and samples were inverted several times prior to overnight incubation at -20 °C. RNA was pelleted by centrifugation at 20,800 x g for 15 min at 4 °C, washed once with 70 % ethanol and shortly air-dried prior to resuspension in 40 µl RNAse-free water.

**Quantitative PCR Analysis**

For one-step qRT-PCR, 3 µl of extracted RNA were mixed 15 µl qPCR mix (qPCRBIO Probe 1-Step Go Lo-ROX, PCR Biosystems) according to manufacturer's protocol. All samples were analysed in triplicates. The following primers and probes were used: GADD34-For: 5' – CAG AAA CCC CTA CTC ATG ATC C – 3'; GADD34-Rev: 5' – AAA TGG ACA GTG ACC TTC TCG – 3'; GADD34-Probe: 5'-6 – FAM – CCCCTAAAGGCCAGAAAGGTGCGC – TAMRA – 3'; GAPDH-For: 5' – GAA GGT GAA GGT CGG AGT C – 3', GAPDH-Rev: 5' – GAA GAT GGT GAT GGG ATT TC – 3'; GAPDH-Probe: 5' – VIC – CAA GCT TCC CGT TCT CAG CCT – TAMRA – 3'; Firefly-Luciferase-For: 5' – CCC TGG TTC CTG GAA CAA TT –

3'; Firefly-Luciferase-Rev: 5' – ATA GCT TCT GCC AAC CGA AC – 3', Firefly-Luciferase-Probe: 5' – Cy5 – ATC GAG GTG GAC ATC ACT TAC GCT – BHQ3 – 3'; Beta-Globin-For: 5' – GAA GGC TCA TGG CAA GAA GG – 3', Beta-Globin-Rev: 5' – ATG ATG AGA CAG CAC AAT AAC CAG – 3', Beta-Globin-Probe: 5' – 6-FAM – ACA AGC TGC ACG TGG ATC CTG AGA A – BHQ1 – 3'. For absolute quantification of GAPDH, GADD34 and *firefly* luciferase copies, a 1:10 serial dilution of purified *in vitro* transcripts was applied. Samples were analysed using a Bio-Rad CFX96 Touch Real-Time PCR detection system using the following cycling protocol: 50 °C 10 min, 95 °C 1 min, 95 °C 10 sec, 60 °C 1 min; steps 3 – 4 repeated for 39 times.

For two step RT-PCR, RNA was reverse transcribed using the High Capacity cDNA Reverse Transcription kit as recommended by the manufacturer (Applied Biosystems) (25 °C 10 min, 37 °C 2 h, 85 °C 5 min). For the detection of GADD34 pre-mRNA, any residual genomic DNA was removed by additional treatment with 4 U TURBO DNAse prior to reverse transcription for 30 min at 37 °C. Digested RNA sample were purified using the NucleoSpin RNA plus kit (Macherey Nagel) prior to cDNA synthesis. cDNA was diluted 1:20 in RNase-free $H_2O$ and 3 µl dilution were used for qRT-PCR analysis using iTaq Universal SYBR Green (Bio-Rad) according to manufacturer's recommendation. The following primers were used: GADD34-Pre-mRNA-For: 5' – ACA GTG ACA GGC AAG TGA CTA G – 3'; GADD34-Pre-mRNA-Rev: 5' – GGA AGA GAG AGA GAG AAG CAA AC – 3'; GAPDH-For: 5' – GAA GGT GAA GGT CGG AGT C – 3', GAPDH-Rev: 5' – GAA GAT GGT GAT GGG ATT TC – 3'; Beta-Globin-For: 5' – GAA GGC TCA TGG CAA GAA GG – 3', Beta-Globin-Rev: 5' – ATG ATG AGA CAG CAC AAT AAC CAG – 3'. Triplicate samples were analyzed using the following cycling protocol: 95 °C 3 min, 95 °C 10 sec, 60 °C 30 sec; steps 2-3 repeated 44 times.

For the analysis of GADD34, GAPDH and *firefly* luciferase transcript abundance, absolute RNA copy numbers were calculated with the help of a standard curve. To calculate the relative abundance of GADD34 mRNA, GADD34 copy numbers were normalized to GAPDH copy numbers as a housekeeping gene control. For the initial calculation of GADD34 and GAPDH mRNA half-lives (Figure 1A), GADD34 / GAPDH RNA copy numbers were normalized to the copy numbers of spiked *firefly* luciferase transcripts to account for RNA loss during purification. As GAPDH levels did not significantly change over the course of the experiment, GADD34 RNA copies were normalized to GAPDH RNA copies in all subsequent RNA half-life panels. The relative abundance of the β-globin RNA and GADD34 pre-mRNA was calculated using the ΔCT method. CT values were normalized to GAPDH and are depicted as fold T0. The analysis of RNA enrichment following protein-RNA co-IP was performed as follows: CT values of GADD34 or β-globin reporter mRNA were log transformed ($1/2^{CT}$) and total RNA copies of spiked *firefly* luciferase *in vitro* transcript were used to account for RNA loss during purification. To account for differences in IP efficiency, values from the precipitated fractions (IP) were further normalised to the absolute protein signal intensities measured in the precipitated samples. Normalised values are depicted as IP/Input and fold GFP control.

**SDS-PAGE and Western Blot Analysis**

Cells were washed with ice-cold PBS and lysed by scraping in ice-cold protein lysis buffer (50 mM Tris HCl pH 7.4, 150 mM NaCl, 1 % Triton X-100, 60 mM β-glycerophosphate, 15 mM 4-nitrophenylphosphate, 1 mM $Na_3VO_4$, 1 mM NaF, supplemented with protease inhibitor cocktail (Roche)). Cell lysates were incubated on ice for 30 min and subsequently centrifuged at 20,800 x g, 4 °C for 15 min. Supernatants were transferred in fresh tubes and stored at -80 °C until analysis. Protein concentration was determined using the Protein Assay Dye Reagent Concentrate (Bio-Rad). Forty µg (for the analysis of p-eIF2α, Akt, p38, HSP27) or 100 µg (for the analysis of GADD34, p-Akt, p-p38 and p-HSP27) total protein was mixed with 6x SDS sample buffer (375 mM Tris-HCl pH 6.8, 50 % glycerol, 9 % SDS, 9 % β-mercaptoethanol, 0.03 % bromophenol blue) and loaded onto polyacrylamide gels, followed by standard gel electrophoresis and blotting onto PVDF membranes.

Membranes were blocked in 5 % BSA (protease-free; Sigma Aldrich) or 5 % non-fat dry milk diluted in TBS-T buffer (25 mM Tris-HCl, 150 mM NaCl, 2 mM KCl, pH 7.4, 0.1 % Tween) depending on antibody requirements. The following primary antibodies were applied in the indicated dilutions and incubated overnight at 4 °C : GADD34 (Proteintech, #10449-I-AP; 1:1,000; milk), eIF2α (Cell Signaling, #9722; 1:1,000; milk), p-eIF2α (Cell Signaling, #3398; 1:1,000; BSA), p38 (Cell Signaling, #8690; 1:1,000 milk), p-p38 (Cell Signaling, #4511, 1:1,000; BSA), Akt (Cell Signaling, #4691; 1 : 1,000; milk), HSP27 (Cell Signaling, #2402; 1:1,000; BSA), p-Akt (R&D systems, #AF887; 1:1,000; BSA), p-HSP27 (Cell Signaling, #2401; 1:1,000; BSA), HCV NS5A (HCV NS5A 9E10 was a gift from Charles Rice lab; 1:2,000; milk), GAPDH (Santa Cruz, #sc-365062; 1:5,000; milk), eIF3b (Bethyl Laboratories, #A301-761A; 1:5,000; milk), myc-tag (Cell Signaling, #2276; 1:1,000; milk). Membranes were washed thrice with TBS-T buffer prior to addition of horseradish peroxidase (HRP)-conjugated secondary antibodies diluted in blocking solution (anti-mouse 1:10,000 or anti-rabbit 1:10,000 antibodies; all from Sigma Aldrich) for 1 h at room temperature. Membranes were washed 3 times for 5 min in TBS-T buffer and prior to chemiluminescence detection using Western Lightning chemiluminescent substrate (Perkin Elmer). Chemiluminescence signal was detected with an ECL-Imager (INTAS) and band quantification performed using the LabImage1D software (INTAS). The measured band intensities were normalized to the indicated loading controls and are shown as arbitrary units or fold control. To account for the variation in total signal intensity among repeats, biological repeats that were imaged separately were additionally normalized to the sum of signals from bands of this membrane (Degasperi et al., 2014).

**Phos-tag acrylamide gel analysis**

For the preparation of Phos-tag gels, 8 % acrylamide gels were prepared, adding a final concentration of 70 µM Phos-tag (FUJIFILM Wako Chemicals) and 140 µM $MnCl_2$ to the resolving gel before casting. 100 µg of protein lysate were loaded on the Phos-tag acrylamide gels, which were run in 1x TGS buffer (25mM Tris-HCl pH 8.8, 192 mM glycine, 0.1% SDS in $dH_2O$) at 80 – 120 V for 2 h in the dark. For the preparation of dephosphorylated protein samples, cells were lysed in dephosphorylation buffer (50 mM Tris HCl pH 8.0, 150 mM NaCl, 1 mM $MgCl_2$, 1 mM $MnCl_2$, 1 % NP40, 2 % glycerol, supplemented with cOmplete mini

protease inhibitor cocktail (Roche)). 100 µg cell lysate was mixed with 3,200 U λ protein phosphatase (New England Biolabs) and incubated at 37 °C for 1 h to achieve complete protein dephosphorylation. After electrophoresis, gels were washed in wet blot transfer buffer supplemented with 1 mM EDTA for 10 min, followed by an additional washing step in absence of EDTA. Proteins were then transferred on pre-activated PVDF membranes by wet blot transfer. Membranes were blocked, stained and imaged as described above. For quantification, the signal from the upper, hyper-phosphorylated band as well as the total lane signal were quantified and the ratio of hyper-phosphorylated/total protein was calculated.

**Polysome profiling**

Huh7 cells (1 x $10^6$ in 10-cm dishes) were seeded one day prior to the experiment. Translation was arrested by treatment with 100 µg/ml cycloheximide (Sigma Aldrich) for 10 min at room temperature. Cells were washed with ice-cold PBS supplemented with 100 µg/ml cycloheximide and lysed by scraping in polysome lysis buffer (20 mM Tris-HCl pH 7.4, 5 mM $MgCl_2$, 150 mM NaCl, 1 % Triton X-100, 100 µg/ml cycloheximide, 200 U/ml RNAsin, 1 µl/ml β-mercaptoethanol; supplemented with cOmplete EDTA-free protease inhibitor cocktail (Roche)). Cell lysates were tumbled for 10 min at 4°C and nuclei pelleted by centrifugation at 10,000 x g for 10 min at 4°C. Cell lysate was loaded onto a linear 17.5–50 % sucrose gradient (dissolved in 20 mM Tris-HCl pH 7.5, 5 mM $MgCl_2$, 150 mM NaCl) and separated by ultracentrifugation at 35,000 rpm in a SW60 rotor (Beckman) at 4 °C for 2.5 h. Polysome profiles were recorded by measuring the absorbance at 254 nm using Teledyne ISCO Foxy R1 system in combination with PeakTrak software.

Fractions of approximately 300 µl were collected every 14 seconds. For RNA isolation, fractions were eluted in 300 µl urea buffer (10 mM Tris pH 7.5, 350 mM NaCl, 10 mM EDTA, 1 % SDS and 7 M urea) and spiked with *firefly* luciferase *in vitro* transcript (3 x $10^8$ copies) to account for loss of material during purification. Total RNA was purified by phenol/chloroform/isoamylalcohol precipitation as described above. RNA samples were analyzed on a 1 % agarose gel to distinguish monosomal and polysomal fractions. Abundance of GADD34 mRNA, β-globin reporter mRNA and *firefly* luciferase *in vitro* transcript was measured in each fraction using qPCR as described above. CT values of target RNAs in individual fractions were log transformed ($1/2^{CT}$) and normalized to the *firefly* luciferase spike-in control. For the analysis of individual fractions, normalized values are depicted as percentages of the sum of total RNA measured in all fractions. The polysomal ratio indicates the percentage of target RNA in polysomal fractions compared to the total fractions.

**Immunofluorescence analysis**

Cells were seeded onto glass coverslips one day before drug treatment, washed once with PBS and fixed for 15 min fixed with 4 % paraformaldehyde. Cells were permeabilized with 0.5 % Triton-X in PBS for 5 min, washed with PBS and blocked for 30 min in blocking buffer (5 % horse serum, 5 % sucrose in PBS) to reduce unspecific binding. Antibodies were diluted in blocking buffer and added for 1 h at the following dilutions: eIF3η (Santa Cruz, #sc-16377 and #sc-137214, both 1:500), myc-tag (Cell Signaling Technology,

#2276S, 1:2,000). Cells were washed 3 times for 5 min with PBS. Secondary antibodies (donkey anti-mouse Alexa Fluor 488, donkey anti-goat Alexa Fluor 568; all from Molecular Probes) were diluted 1:2,000 in blocking buffer and used for detection of primary antibodies for 1 h at room temperature. Nuclei were stained with DAPI (1: 10,000 in PBS, Sigma Aldrich) for 3 min prior to washing. Cells were washed twice with PBS and once with $H_2O$. Coverslips were mounted on glass slides using Fluoromount-G mounting medium (SouthernBiotech). Images were acquired on a Nikon Eclipse Ti-E microscope using 20x (N.A. 1.0 PLAN APO λ) or 40x (N.A. 1.3 PLAN Fluor Oil) objectives. For co-localization analysis, samples were imaged on a Leica SP8 TCS DLS confocal microscope using a 63x objective (N.A. 1.4 HC PLAN APO CS2 Oil). Image analysis was performed using the FIJI software package (Schindelin et al., 2012).

**Human phospho-MAPK array**

Kinase arrays were conducted as described in (Roth et al., 2017). Briefly, 400 µg of protein from mock- and HCV-infected Huh7 cells lysed at 72 h post infection or Huh7 cells treated for 1 h with DMSO or thapsigargin were analyzed using the Proteome Profiler Human Phospho-MAPK Array (R&D Systems) as recommended by the manufacturer. Signal was detected on a Vilber-Loumat imager and quantified using Image J software.

**Statistical analysis**

Data from biological repeats is depicted as individual replicates with mean and standard deviation (SD). For experiments using multiple KO and Ctrl cell clones, data points and mean ± SD indicate variance among individual clones. Statistical analysis was performed using GraphPad Prism software, version 8.0.1. For comparison of two datasets, unpaired two-sided Student's t-test was applied, using Welsh's correction if datasets showed unequal variances. For comparison of three or more datasets with one or two variables, unpaired, two-sided one-way or two-way ANOVA was performed, respectively. To compare mRNA stabilities among datasets, statistical significance (ANOVA) over all time points between controls and stressed or KO conditions in indicated. For subsequent multiple comparisons, Dunnett's posttest was applied for testing against a single control. For comparisons between multiple different groups of data, Holm-Sidak's posttest was applied. P values of less than 0.5 were considered statistically significant and are indicated accordingly ($P < 0.05$ = * or $^{+}$, $P < 0.01$ = ** or $^{++}$, $P < 0.001$ = *** or $^{+++}$, $P < 0.0001$ = **** or $^{++++}$).

**References**

Aulas, A., Fay, M.M., Lyons, S.M., Achorn, C.A., Kedersha, N., Anderson, P., and Ivanov, P. (2017). Stress-specific differences in assembly and composition of stress granules and related foci. J Cell Sci *130*, 927-937.

Bakheet, T., Hitti, E., Al-Saif, M., Moghrabi, W.N., and Khabar, K.S.A. (2018). The AU-rich element landscape across human transcriptome reveals a large proportion in introns and regulation by ELAVL1/HuR. Biochim Biophys Acta Gene Regul Mech *1861*, 167-177.

Benjamin, D., Schmidlin, M., Min, L., Gross, B., and Moroni, C. (2006). BRF1 protein turnover and mRNA decay activity are regulated by protein kinase B at the same phosphorylation sites. Mol Cell Biol *26*, 9497-9507.

Brush, M.H., and Shenolikar, S. (2008). Control of cellular GADD34 levels by the 26S proteasome. Molecular and cellular biology *28*, 6989-7000.

Brush, M.H., Weiser, D.C., and Shenolikar, S. (2003). Growth arrest and DNA damage-inducible protein GADD34 targets protein phosphatase 1 alpha to the endoplasmic reticulum and promotes dephosphorylation of the alpha subunit of eukaryotic translation initiation factor 2. Molecular and cellular biology *23*, 1292-1303.

Carballo, E., Lai, W.S., and Blackshear, P.J. (1998). Feedback inhibition of macrophage tumor necrosis factor-alpha production by tristetraprolin. Science *281*, 1001-1005.

Chen, C.Y., Gherzi, R., Ong, S.E., Chan, E.L., Raijmakers, R., Pruijn, G.J., Stoecklin, G., Moroni, C., Mann, M., and Karin, M. (2001). AU binding proteins recruit the exosome to degrade ARE-containing mRNAs. Cell *107*, 451-464.

Chen, C.Y., and Shyu, A.B. (1995). AU-rich elements: characterization and importance in mRNA degradation. Trends Biochem Sci *20*, 465-470.

Chrestensen, C.A., Schroeder, M.J., Shabanowitz, J., Hunt, D.F., Pelo, J.W., Worthington, M.T., and Sturgill, T.W. (2004). MAPKAP kinase 2 phosphorylates tristetraprolin on in vivo sites including Ser178, a site required for 14-3-3 binding. J Biol Chem *279*, 10176-10184.

Ciais, D., Cherradi, N., and Feige, J.J. (2013). Multiple functions of tristetraprolin/TIS11 RNA-binding proteins in the regulation of mRNA biogenesis and degradation. Cell Mol Life Sci *70*, 2031-2044.

Clement, S.L., Scheckel, C., Stoecklin, G., and Lykke-Andersen, J. (2011). Phosphorylation of tristetraprolin by MK2 impairs AU-rich element mRNA decay by preventing deadenylase recruitment. Mol Cell Biol *31*, 256-266.

Cook, K.B., Kazan, H., Zuberi, K., Morris, Q., and Hughes, T.R. (2011). RBPDB: a database of RNA-binding specificities. Nucleic Acids Res *39*, D301-308.

Darnell, J.E., Jr. (1982). Variety in the level of gene control in eukaryotic cells. Nature *297*, 365-371.

Degasperi, A., Birtwistle, M.R., Volinsky, N., Rauch, J., Kolch, W., and Kholodenko, B.N. (2014). Evaluating strategies to normalise biological replicates of Western blot data. PLoS One *9*, e87293.

Fallmann, J., Sedlyarov, V., Tanzer, A., Kovarik, P., and Hofacker, I.L. (2016). AREsite2: an enhanced database for the comprehensive investigation of AU/GU/U-rich elements. Nucleic Acids Res *44*, D90-95.

Fan, X.C., and Steitz, J.A. (1998). Overexpression of HuR, a nuclear-cytoplasmic shuttling protein, increases the in vivo stability of ARE-containing mRNAs. EMBO J *17*, 3448-3460.

Fawcett, T.W., Martindale, J.L., Guyton, K.Z., Hai, T., and Holbrook, N.J. (1999). Complexes containing activating transcription factor (ATF)/cAMP-responsive-element-binding protein (CREB) interact with the CCAAT/enhancer-binding protein (C/EBP)-ATF composite site to regulate Gadd153 expression during the stress response. The Biochemical journal *339 ( Pt 1)*, 135-141.

Fukao, A., and Fujiwara, T. (2017). The coupled and uncoupled mechanisms by which trans-acting factors regulate mRNA stability and translation. J Biochem *161*, 309-314.

Gaba, A., Jacobson, A., and Sachs, M.S. (2005). Ribosome occupancy of the yeast CPA1 upstream open reading frame termination codon modulates nonsense-mediated mRNA decay. Molecular cell *20*, 449-460.

Gambardella, G., Staiano, L., Moretti, M.N., De Cegli, R., Fagnocchi, L., Di Tullio, G., Polletti, S., Braccia, C., Armirotti, A., Zippo, A.*, et al.* (2020). GADD34 is a modulator of autophagy during starvation. Sci Adv *6*.

Gao, M., Wilusz, C.J., Peltz, S.W., and Wilusz, J. (2001). A novel mRNA-decapping activity in HeLa cytoplasmic extracts is regulated by AU-rich elements. The EMBO journal *20*, 1134-1143.

Garcia-Maurino, S.M., Rivero-Rodriguez, F., Velazquez-Cruz, A., Hernandez-Vellisca, M., Diaz-Quintana, A., De la Rosa, M.A., and Diaz-Moreno, I. (2017). RNA Binding Protein Regulation and Cross-Talk in the Control of AU-rich mRNA Fate. Front Mol Biosci *4*, 71.

Harding, H.P., Novoa, I., Zhang, Y., Zeng, H., Wek, R., Schapira, M., and Ron, D. (2000). Regulated translation initiation controls stress-induced gene expression in mammalian cells. Mol Cell *6*, 1099-1108.

Hinnebusch, A.G. (2011). Molecular mechanism of scanning and start codon selection in eukaryotes. Microbiol Mol Biol Rev *75*, 434-467, first page of table of contents.

Holczer, M., Banhegyi, G., and Kapuy, O. (2016). GADD34 Keeps the mTOR Pathway Inactivated in Endoplasmic Reticulum Stress Related Autophagy. PloS one *11*, e0168359.

Hollander, M.C., Zhan, Q., Bae, I., and Fornace, A.J., Jr. (1997). Mammalian GADD34, an apoptosis- and DNA damage-inducible gene. The Journal of biological chemistry *272*, 13731-13737.

Ito, S., Tanaka, Y., Oshino, R., Aiba, K., Thanasegaran, S., Nishio, N., and Isobe, K. (2015). GADD34 inhibits activation-induced apoptosis of macrophages through enhancement of autophagy. Scientific reports *5*, 8327.

Jackman, J., Alamo, I., Jr., and Fornace, A.J., Jr. (1994). Genotoxic stress confers preferential and coordinate messenger RNA stability on the five gadd genes. Cancer research *54*, 5656-5662.

Johnson, B.A., Geha, M., and Blackwell, T.K. (2000). Similar but distinct effects of the tristetraprolin/TIS11 immediate-early proteins on cell survival. Oncogene *19*, 1657-1664.

Johnson, B.A., Stehn, J.R., Yaffe, M.B., and Blackwell, T.K. (2002). Cytoplasmic localization of tristetraprolin involves 14-3-3-dependent and -independent mechanisms. J Biol Chem *277*, 18029-18036.

Jousse, C., Oyadomari, S., Novoa, I., Lu, P., Zhang, Y., Harding, H.P., and Ron, D. (2003). Inhibition of a constitutive translation initiation factor 2alpha phosphatase, CReP, promotes survival of stressed cells. J Cell Biol *163*, 767-775.

Kedersha, N., Stoecklin, G., Ayodele, M., Yacono, P., Lykke-Andersen, J., Fritzler, M.J., Scheuner, D., Kaufman, R.J., Golan, D.E., and Anderson, P. (2005). Stress granules and processing bodies are dynamically linked sites of mRNP remodeling. J Cell Biol *169*, 871-884.

Klein, P., Kallenberger, S.M., Roth, H., Roth, K., Ly-Hartig, T.B.N., Magg, V., Ales, J., Talemi, S.R., Qiang, Y., Wolf, S.*, et al.* (2022). Temporal control of the integrated stress response by a stochastic molecular switch. Sci Adv *8*, eabk2022.

Kontoyiannis, D., Pasparakis, M., Pizarro, T.T., Cominelli, F., and Kollias, G. (1999). Impaired on/off regulation of TNF biosynthesis in mice lacking TNF AU-rich elements: implications for joint and gut-associated immunopathologies. Immunity *10*, 387-398.

Kumar, S., Jiang, M.S., Adams, J.L., and Lee, J.C. (1999). Pyridinylimidazole compound SB 203580 inhibits the activity but not the activation of p38 mitogen-activated protein kinase. Biochem Biophys Res Commun *263*, 825-831.

Lai, W.S., Carballo, E., Thorn, J.M., Kennington, E.A., and Blackshear, P.J. (2000). Interactions of CCCH zinc finger proteins with mRNA. Binding of tristetraprolin-related zinc finger proteins to Au-rich elements and destabilization of mRNA. The Journal of biological chemistry *275*, 17827-17837.

Lali, F.V., Hunt, A.E., Turner, S.J., and Foxwell, B.M. (2000). The pyridinyl imidazole inhibitor SB203580 blocks phosphoinositide-dependent protein kinase activity, protein kinase B phosphorylation, and retinoblastoma hyperphosphorylation in interleukin-2-stimulated T cells independently of p38 mitogen-activated protein kinase. J Biol Chem *275*, 7395-7402.

Lee, J.E., Morrison, W., and Hollien, J. (2018). Hairy and enhancer of split 1 (HES1) protects cells from endoplasmic reticulum stress-induced apoptosis through repression of GADD34. J Biol Chem *293*, 5947-5955.

Lee, Y.Y., Cevallos, R.C., and Jan, E. (2009). An upstream open reading frame regulates translation of GADD34 during cellular stresses that induce eIF2alpha phosphorylation. J Biol Chem *284*, 6661-6673.

Leppek, K., Schott, J., Reitter, S., Poetz, F., Hammond, M.C., and Stoecklin, G. (2013). Roquin promotes constitutive mRNA decay via a conserved class of stem-loop recognition motifs. Cell *153*, 869-881.

Lykke-Andersen, J., and Wagner, E. (2005). Recruitment and activation of mRNA decay enzymes by two ARE-mediated decay activation domains in the proteins TTP and BRF-1. Genes Dev *19*, 351-361.

Ma, Y., and Hendershot, L.M. (2003). Delineation of a negative feedback regulatory loop that controls protein translation during endoplasmic reticulum stress. The Journal of biological chemistry *278*, 34864-34873.

Mahmoud, L., Moghrabi, W., Khabar, K.S.A., and Hitti, E.G. (2019). Bi-phased regulation of the post-transcriptional inflammatory response by Tristetraprolin levels. RNA Biol *16*, 309-319.

Maitra, S., Chou, C.F., Luber, C.A., Lee, K.Y., Mann, M., and Chen, C.Y. (2008). The AU-rich element mRNA decay-promoting activity of BRF1 is regulated by mitogen-activated protein kinase-activated protein kinase 2. RNA *14*, 950-959.

Marciniak, S.J., Yun, C.Y., Oyadomari, S., Novoa, I., Zhang, Y., Jungreis, R., Nagata, K., Harding, H.P., and Ron, D. (2004). CHOP induces death by promoting protein synthesis and oxidation in the stressed endoplasmic reticulum. Genes & development *18*, 3066-3077.

Moore, M.J., Blachere, N.E., Fak, J.J., Park, C.Y., Sawicka, K., Parveen, S., Zucker-Scharff, I., Moltedo, B., Rudensky, A.Y., and Darnell, R.B. (2018). ZFP36 RNA-binding proteins restrain T cell activation and anti-viral immunity. Elife *7*.

Mukherjee, D., Gao, M., O'Connor, J.P., Raijmakers, R., Pruijn, G., Lutz, C.S., and Wilusz, J. (2002). The mammalian exosome mediates the efficient degradation of mRNAs that contain AU-rich elements. EMBO J *21*, 165-174.

Mukherjee, N., Jacobs, N.C., Hafner, M., Kennington, E.A., Nusbaum, J.D., Tuschl, T., Blackshear, P.J., and Ohler, U. (2014). Global target mRNA specification and regulation by the RNA-binding protein ZFP36. Genome Biol *15*, R12.

Murata, T., Morita, N., Hikita, K., Kiuchi, K., Kiuchi, K., and Kaneda, N. (2005). Recruitment of mRNA-destabilizing protein TIS11 to stress granules is mediated by its zinc finger domain. Exp Cell Res *303*, 287-299.

Novoa, I., Zeng, H., Harding, H.P., and Ron, D. (2001). Feedback inhibition of the unfolded protein response by GADD34-mediated dephosphorylation of eIF2alpha. The Journal of cell biology *153*, 1011-1022.

Novoa, I., Zhang, Y., Zeng, H., Jungreis, R., Harding, H.P., and Ron, D. (2003). Stress-induced gene expression requires programmed recovery from translational repression. EMBO J *22*, 1180-1187.

Ozgur, S., Chekulaeva, M., and Stoecklin, G. (2010). Human Pat1b connects deadenylation with mRNA decapping and controls the assembly of processing bodies. Molecular and cellular biology *30*, 4308-4323.

Pakos-Zebrucka, K., Koryga, I., Mnich, K., Ljujic, M., Samali, A., and Gorman, A.M. (2016). The integrated stress response. EMBO Rep *17*, 1374-1395.

Piecyk, M., Wax, S., Beck, A.R., Kedersha, N., Gupta, M., Maritim, B., Chen, S., Gueydan, C., Kruys, V., Streuli, M.*, et al.* (2000). TIA-1 is a translational silencer that selectively regulates the expression of TNF-alpha. The EMBO journal *19*, 4154-4163.

Riggs, C.L., Kedersha, N., Ivanov, P., and Anderson, P. (2020). Mammalian stress granules and P bodies at a glance. J Cell Sci *133*.

Roth, H., Magg, V., Uch, F., Mutz, P., Klein, P., Haneke, K., Lohmann, V., Bartenschlager, R., Fackler, O.T., Locker, N.*, et al.* (2017). Flavivirus Infection Uncouples Translation Suppression from Cellular Stress Responses. mBio *8*.

Ruggieri, A., Dazert, E., Metz, P., Hofmann, S., Bergeest, J.P., Mazur, J., Bankhead, P., Hiet, M.S., Kallis, S., Alvisi, G.*, et al.* (2012). Dynamic oscillation of translation and stress granule formation mark the cellular response to virus infection. Cell Host Microbe *12*, 71-85.

Rutkowski, D.T., Arnold, S.M., Miller, C.N., Wu, J., Li, J., Gunnison, K.M., Mori, K., Sadighi Akha, A.A., Raden, D., and Kaufman, R.J. (2006). Adaptation to ER stress is mediated by differential stabilities of pro-survival and pro-apoptotic mRNAs and proteins. PLoS biology *4*, e374.

Sandler, H., Kreth, J., Timmers, H.T., and Stoecklin, G. (2011). Not1 mediates recruitment of the deadenylase Caf1 to mRNAs targeted for degradation by tristetraprolin. Nucleic Acids Res *39*, 4373-4386.

Schindelin, J., Arganda-Carreras, I., Frise, E., Kaynig, V., Longair, M., Pietzsch, T., Preibisch, S., Rueden, C., Saalfeld, S., Schmid, B.*, et al.* (2012). Fiji: an open-source platform for biological-image analysis. Nat Methods *9*, 676-682.

Schmidlin, M., Lu, M., Leuenberger, S.A., Stoecklin, G., Mallaun, M., Gross, B., Gherzi, R., Hess, D., Hemmings, B.A., and Moroni, C. (2004). The ARE-dependent mRNA-destabilizing activity of BRF1 is regulated by protein kinase B. EMBO J *23*, 4760-4769.

Schott, J., and Stoecklin, G. (2010). Networks controlling mRNA decay in the immune system. Wiley Interdiscip Rev RNA *1*, 432-456.

Stoecklin, G., Colombi, M., Raineri, I., Leuenberger, S., Mallaun, M., Schmidlin, M., Gross, B., Lu, M., Kitamura, T., and Moroni, C. (2002). Functional cloning of BRF1, a regulator of ARE-dependent mRNA turnover. EMBO J *21*, 4709-4718.

Stoecklin, G., Lu, M., Rattenbacher, B., and Moroni, C. (2003). A constitutive decay element promotes tumor necrosis factor alpha mRNA degradation via an AU-rich element-independent pathway. Mol Cell Biol *23*, 3506-3515.

Stoecklin, G., Mayo, T., and Anderson, P. (2006). ARE-mRNA degradation requires the 5'-3' decay pathway. EMBO reports *7*, 72-77.

Stoecklin, G., Stubbs, T., Kedersha, N., Wax, S., Rigby, W.F., Blackwell, T.K., and Anderson, P. (2004a). MK2-induced tristetraprolin:14-3-3 complexes prevent stress granule association and ARE-mRNA decay. EMBO J *23*, 1313-1324.

Stoecklin, G., Stubbs, T., Kedersha, N., Wax, S., Rigby, W.F., Blackwell, T.K., and Anderson, P. (2004b). MK2-induced tristetraprolin:14-3-3 complexes prevent stress granule association and ARE-mRNA decay. The EMBO journal *23*, 1313-1324.

Tan, F.E., and Elowitz, M.B. (2014). Brf1 posttranscriptionally regulates pluripotency and differentiation responses downstream of Erk MAP kinase. Proc Natl Acad Sci U S A *111*, E1740-1748.

Taniuchi, S., Miyake, M., Tsugawa, K., Oyadomari, M., and Oyadomari, S. (2016). Integrated stress response of vertebrates is regulated by four eIF2alpha kinases. Sci Rep *6*, 32886.

Taylor, G.A., Thompson, M.J., Lai, W.S., and Blackshear, P.J. (1995). Phosphorylation of tristetraprolin, a potential zinc finger transcription factor, by mitogen stimulation in intact cells and by mitogen-activated protein kinase in vitro. J Biol Chem *270*, 13341-13347.

Tchen, C.R., Brook, M., Saklatvala, J., and Clark, A.R. (2004). The stability of tristetraprolin mRNA is regulated by mitogen-activated protein kinase p38 and by tristetraprolin itself. J Biol Chem *279*, 32393-32400.

Tiedje, C., Ronkina, N., Tehrani, M., Dhamija, S., Laass, K., Holtmann, H., Kotlyarov, A., and Gaestel, M. (2012). The p38/MK2-driven exchange between tristetraprolin and HuR regulates AU-rich element-dependent translation. PLoS Genet *8*, e1002977.

Wang, X.Z., and Ron, D. (1996). Stress-induced phosphorylation and activation of the transcription factor CHOP (GADD153) by p38 MAP Kinase. Science *272*, 1347-1349.

Wilusz, C.J., Wormington, M., and Peltz, S.W. (2001). The cap-to-tail guide to mRNA turnover. Nat Rev Mol Cell Biol *2*, 237-246.

Worthington, M.T., Pelo, J.W., Sachedina, M.A., Applegate, J.L., Arseneau, K.O., and Pizarro, T.T. (2002). RNA binding properties of the AU-rich element-binding recombinant Nup475/TIS11/tristetraprolin protein. J Biol Chem *277*, 48558-48564.

Xu, L., Chen, S., and Bergan, R.C. (2006). MAPKAPK2 and HSP27 are downstream effectors of p38 MAP kinase-mediated matrix metalloproteinase type 2 activation and cell invasion in human prostate cancer. Oncogene *25*, 2987-2998.

Yang, E., van Nimwegen, E., Zavolan, M., Rajewsky, N., Schroeder, M., Magnasco, M., and Darnell, J.E., Jr. (2003). Decay rates of human mRNAs: correlation with functional characteristics and sequence attributes. Genome Res *13*, 1863-1872.

Young, S.K., Willy, J.A., Wu, C., Sachs, M.S., and Wek, R.C. (2015). Ribosome Reinitiation Directs Gene-specific Translation and Regulates the Integrated Stress Response. J Biol Chem *290*, 28257-28271.

Zhang, W., Wagner, B.J., Ehrenman, K., Schaefer, A.W., DeMaria, C.T., Crater, D., DeHaven, K., Long, L., and Brewer, G. (1993). Purification, characterization, and cDNA cloning of an AU-rich element RNA-binding protein, AUF1. Mol Cell Biol *13*, 7652-7665.

Zhao, W., Liu, M., D'Silva, N.J., and Kirkwood, K.L. (2011). Tristetraprolin regulates interleukin-6 expression through p38 MAPK-dependent affinity changes with mRNA 3' untranslated region. J Interferon Cytokine Res *31*, 629-637.

Zhao, Y.Y., Tian, Y., Zhang, J., Xu, F., Yang, Y.P., Huang, Y., Zhao, H.Y., Zhang, J.W., Xue, C., Lam, M.H., *et al.* (2014). Effects of an oral allosteric AKT inhibitor (MK-2206) on human nasopharyngeal cancer in vitro and in vivo. Drug Des Devel Ther *8*, 1827-1837.

Zhou, W., Brush, M.H., Choy, M.S., and Shenolikar, S. (2011). Association with endoplasmic reticulum promotes proteasomal degradation of GADD34 protein. J Biol Chem *286*, 21687-21696.

Zhou, W., Jeyaraman, K., Yusoff, P., and Shenolikar, S. (2013). Phosphorylation at tyrosine 262 promotes GADD34 protein turnover. The Journal of biological chemistry *288*, 33146-33155.

Zhu, W., Brauchle, M.A., Di Padova, F., Gram, H., New, L., Ono, K., Downey, J.S., and Han, J. (2001). Gene suppression by tristetraprolin and release by the p38 pathway. Am J Physiol Lung Cell Mol Physiol *281*, L499-508.

Zubiaga, A.M., Belasco, J.G., and Greenberg, M.E. (1995). The nonamer UUAUUUAUU is the key AU-rich sequence motif that mediates mRNA degradation. Mol Cell Biol *15*, 2219-2230.

Zufferey, R., Nagy, D., Mandel, R.J., Naldini, L., and Trono, D. (1997). Multiply attenuated lentiviral vector achieves efficient gene delivery in vivo. Nat Biotechnol *15*, 871-875.

## Figure legends

**Figure 1. GADD34 3' UTR contains an RNA destabilizing AU-rich element (ARE). (A)** Measurement of basal GADD34 mRNA decay. Levels of GADD34 and GAPDH mRNAs following actinomycin D chase were determined by qRT-PCR and normalized to a *firefly* luciferase RNA spike-in. GADD34 and GAPDH mRNA half-lives ($t_{1/2}$) were calculated using a semi-logarithmic curve fitting. Shown are means ± SD of biological replicates (n=3). **(B)** Decay measurements in cells infected with HCV for 48 h and subsequently treated with IFN-$\alpha$ for 24 h (left panel) or transfected with double-stranded RNA (right panel) for 16 h prior to actinomycin D chase (n=3). GADD34 mRNA levels were normalized to stable GAPDH transcripts and mRNA half-lives calculated as in (A). **(C)** Decay measurements in cells treated with thapsigargin (Thap) for up to 12 h or solvent control (DMSO) prior to 2-hour actinomycin D chase (n=3). **(D)** Ribonucleotide sequence of the 3' UTR of the human GADD34 mRNA. Wild type sequence is displayed on the top ($GADD34_{WT}$). Sequence with mutated pentamers is displayed on the bottom ($GADD34_{MUT}$). Purple box, ARE; AUUUA, ZFP36/TTP pentameric recognition motif; AAUAAA, polyA signal. **(E)** Schematics of the different $\beta$-globin reporter mRNAs. GADD34 or $GADD34_{MUT}$ 3' UTR was inserted upstream of the $\beta$-globin 3' UTR. The ARE of TNF-$\alpha$ served as a positive control. **(F)** $\beta$-globin reporter mRNA stability in stable cell lines. Half-lives were measured as described in (B) (n=3). Statistical significance compared to WT $\beta$-globin reporter mRNA is indicated. **(G)** Measurement of basal GADD34 mRNA expression levels in Ctrl and

GADD34ΔARE (ΔARE) cell clones. Values were normalised to GAPDH mRNA levels. Bars show a representative mean ± SD of three Ctrl and three ΔARE individual cell clones (n=2). **(H)** GADD34 mRNA expression levels in Ctrl and ΔARE clonal cell lines after treatment with thapsigargin. Values were normalised to GAPDH mRNA levels and are depicted as fold DMSO controls. Histograms show the mean ± SD of three Ctrl and three ΔARE individual cell clones (n=1). **(I)** GADD34 mRNA decay in Ctrl and ΔARE cell clones. Cells were treated with thapsigargin or DMSO control for up to 6 h prior to addition of actinomycin D. Shown is the mean ± SD of three Ctrl and three ΔARE individual cell clones (n=1).

**Figure 2. The RNA-binding proteins TTP and Brf1 specifically bind to GADD34 mRNA ARE. (A)** Myc-his-tagged GFP, TTP, Brf1, TTP murine orthologue (msTTP) or RNA-binding mutant ($msTTP_{m1,2}$) were immunoprecipitated using Ni-NTA beads from transiently expressing cells. RNA was subsequently isolated and analyzed by qRT-PCR (RNA-IP) (n=3). Upper panel: representative Western blot analysis (n=3). Shown are input cell extracts (10% of total, input) and immunoprecipitated proteins (50% of eluate, IP). Proteins were detected using an anti-myc antibody. Middle and bottom panels: Analysis of co-precipitated GADD34 and GAPDH mRNAs, normalized to GFP control. Statistical significance compared to GFP is indicated. **(B)** Myc-his-tagged GFP, TTP, Brf1, TTP murine orthologue (msTTP) or RNA-binding mutant ($msTTP_{m1,2}$) were transiently expressed in the β-globin reporter cell lines (β-glo WT, β-glo GADD34, β-glo $GADD34_{MUT}$) and RNA-IP performed as described in (A) (n=3). Upper panel: representative Western blot analysis of input and immunoprecipitated fractions. Expression of eIF3b served as loading control. Middle and bottom panels: quantification of co-precipitated β-globin reporter mRNAs, normalized to GFP. *, statistical significance compared to β-glo WT cells. $^{+}$, statistical significance compared to β-glo GADD34 cells.

**Figure 3. Overexpression of TTP and Brf1 induces GADD34 mRNA destabilization during stress recovery.** Cells transiently expressing myc-his-tagged GFP, TTP, Brf1, msTTP or $msTTP_{m1,2}$ were treated with thapsigargin for the indicated times or with solvent control (0 h). **(A)** Quantification of p-eIF2α (upper panel) and GADD34 (bottom panel) protein abundance (related to Figure S3B). Measured band intensity values were normalized to eIF3b and are depicted as arbitrary units (a.u.). Shown are means ± SD (n=3). Statistical significance compared to GFP at each time point is indicated. **(B)** Quantification of GADD34 mRNA expression levels by qRT-PCR. GADD34 mRNA levels were normalized to GAPDH values and are represented as fold of DMSO values (n=3). Statistical significance compared to GFP at each time point is indicated. **(C)** GADD34 mRNA decay in cells treated with thapsigargin or solvent control (DMSO) for the indicated times prior to actinomycin D chase. Levels of GADD34 mRNA were normalized to stable GAPDH transcripts and are plotted as percentage of the initial time point. Shown are mean ± SD (n=3). Statistical significance over all time points compared to GFP is indicated.

**Figure 4. Stress-mediated activation of the p38-MAPK/MK2 and PI3K/Akt signaling pathways mediates TTP and Brf1 phosphorylation. (A)** Analysis of p38-MAPK/MK2 and PI3K/Akt kinase signaling pathways after HCV infection. Cells were infected with HCV for 48 h prior to the addition of IFN-α. At 72 h post infection, cell lysates were analyzed by Western blot (n=3). **(B)** Quantifications corresponding to *(a)*. Measured band intensities were normalized to eIF3b and are depicted as arbitrary units (a.u.). Shown are means ± SD (n=3). Statistical significance compared to Mock is indicated. **(C)** Dynamics of p38-MAPK/MK2 and PI3K/Akt pathway activation in thapsigargin-treated. Cells were treated with thapsigargin or DMSO control for up to 6 h prior to Western blot analysis (n=3). **(D)** Quantifications corresponding to (C). Analysis as in (B). Shown are means ± SD from n=3 independent biological repeats. Statistical significance compared to T0 (DMSO) is indicated. **(E and F)** Analysis of TTP *(e)* and Brf1 *(f)* phosphorylation forms by Phos-tag acrylamide gel. Cells transiently expressing myc-his-tagged TTP or Brf1 were treated with thapsigargin or solvent control (0 h, DMSO) for the indicated times. Cell extracts digested with lambda phosphatase (λPPase) were used to determine the migration pattern of unphosphorylated forms. H, hyper-phosphorylated form. U, unphosphorylated form. Shown are representative Western blot analyses (left panels) and corresponding quantifications (right panels). Signal intensities of the hyper-phosphorylated forms are depicted as percentage of the total signal in the corresponding lane. All mean ± SD of (n=3). Statistical significance compared to T0 (DMSO) is indicated.

**Figure 5. Increased basal GADD34 expression in DKO cells. (A)** GADD34 mRNA expression in TTP and Brf1 single KO cell clones. GADD34 mRNA levels were normalized to GAPDH mRNA levels. Shown is a representative mean ± SD of all individual cell clones (n=2). **(B toE)** GADD34 mRNA decay measurements in single KO clones. Three Ctrl, four TTP and five Brf1 cell clones were treated with DMSO (B and C) or thapsigargin (D and E) for 3 h prior to the addition of actinomycin D. Shown is the mean ± SD of all individual cell clones (n=1). Statistical significance over all time points compared to Ctrl clones is indicated. **(F)** GADD34 mRNA expression in TTP-Brf1 double KO (DKO) cell clones. GADD34 mRNA levels were normalized to GAPDH mRNA levels. Shown is a representative mean ± SD of all individual cell clones (n=2). **(G and H)** GADD34 mRNA decay measurements in DKO clones. Three Ctrl and five DKO cell clones were treated with DMSO (G) or thapsigargin (H) for 3 h prior to the addition of actinomycin D. Shown is the mean ± SD of all individual cell clones (n=1). Statistical significance over all time points compared to Ctrl clones is indicated. **(I and J)** Analysis of GADD34 and p-eIF2α expression levels in Ctrl and DKO cell clones under normal conditions (n=2). (I) Representative Western blot analysis. (J) Corresponding quantifications of GADD34 (left panel) and p-eIF2α (right panel) protein abundance. Measured band intensities were normalized to eIF3b and are depicted as arbitrary units (a.u.). Shown is a representative mean of all clones ± SD. Statistical significance compared to Ctrl clones is indicated. **(K and L)** Analysis of GADD34 and p-eIF2α expression levels in Ctrl and DKO cell clones upon thapsigargin treatment (n=2). (K) Representative analysis for Ctrl clone #1 and DKO clones #9 and #18. (L) Representative quantification of GADD34 protein

abundance in all Ctrl and DKO cell clones (n=2). Shown is the mean ± SD of all individual clones. Statistical significance compared to Ctrl cell clones at the respective time point is indicated.

**Figure 6. DKO cell clone reduced responsiveness to stress mirrors chronically stressed cells. (A)** Analysis of stress responsiveness to increasing doses of arsenite in Ctrl and DKO cells. The ability of cells to form SGs was assessed by immunofluorescence analysis (related to Figure S 9). Shown is a representative mean percentage of SG-positive cells ± SD of all individual clones (n=2). Statistical significance compared to Ctrl cell clones at the respective doses is indicated. **(B to D)** Ctrl and DKO cell clones were treated with thapsigargin for 6 or 12 h or solvent control (0 h) before addition of a second stress pulse of high-dose arsenite for 45 minutes (acute stress, AS). (B) Schematics of the experimental design (upper panel) and representative Western blot analysis of Ctrl #5 and DKO #18 cell clones (lower panel). (C) Quantification of p-eIF2α levels in all clones. Measured band intensities were normalized to eIF3b and are depicted as arbitrary units (a.u.). Shown are representative means ± SD of all Ctrl and DKO individual cell clones (n=2). Statistical significance compared to cells in the absence of AS is indicated. (D) Analysis of SG formation in all individual Ctrl and DKO cell clones (related to Figure S6B). Shown is a representative mean percentage of SG-positive cells ± SD of all individual clones (n=2). Statistical significance compared to Ctrl cell clones at the respective time point is indicated. **(E to G)** Chronically stressed (+CS) Ctrl or unstressed (-CS) Ctrl and DKO cell clones were subjected to a pulse of acute arsenite stress (AS). (E) Schematics of the experimental design (upper panel) and representative Western blot analysis of Ctrl #5 and DKO #18 cell clones (lower panel) (n=2). (F) Quantifications of p-eIF2α (upper panel) and GADD34 (lower panel) protein mean abundance ± SD in **e** including all individual cell clones (n=2). (G) Analysis of SG formation in unstressed (-CS) Ctrl and DKO or chronically stressed (+CS) Ctrl cell clones after treatment with acute arsenite stress (AS) (related to Figure S6F). Shown is a representative analysis of mean percentage of SG-positive cells ± SD of all individual cell clones (n=2). Statistical significance compared to Ctrl (-CS) is indicated.

**Figure 7. Proposed model: GADD34 levels act as a molecular memory of the ISR.** Top panel: Exposure to an acute stress pulse results in phosphorylation of eIF2α and activation of the ISR, as well as inhibition of TTP and Brf1 decay activity by phosphorylation. Consequently, GADD34 mRNA synthesis is amplified by the stabilization of pre-existing mRNA, allowing a rapid increase in GADD34 levels and efficient dephosphorylation of eIF2α. Upon stress release, TTP and Brf1 are progressively dephosphorylated and regain their decay activity, destabilizing GADD34 mRNA. Elevated GADD34 mRNA levels act as a molecular memory of the previously activated ISR. Cells regain full responsiveness to stress once GADD34 mRNA turnover returns to its initial rate and levels return to baseline. Middle panel: Cells subjected to a second acute stress pulse during the recovery period show attenuated responsiveness to stress due to sustained GADD34 mRNA levels, which counteract eIF2α phosphorylation. Bottom panel: Cells exposed

to chronic low-dose stress show increased basal levels of GADD34 and reduced stress responsiveness, resembling that observed in GADD34 ΔARE and TTP-Brf1 DKO context.

# Figure 1

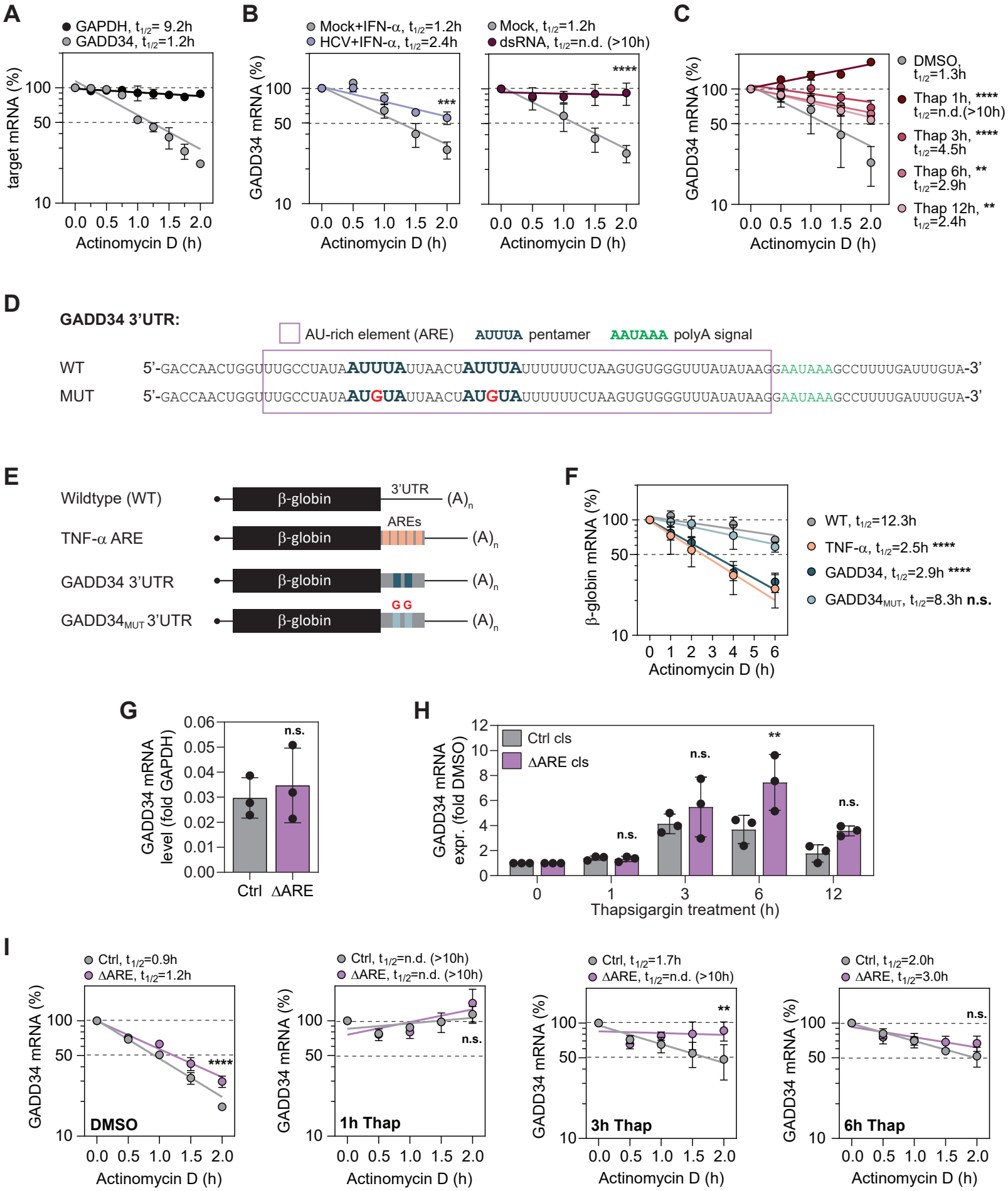
A
GAPDH, t1/2= 9.2h
GADD34, t1/2=1.2h
target mRNA (%)
Actinomycin D (h)
B
Mock+IFN-α, t1/2=1.2h
HCV+IFN-α, t1/2=2.4h
Mock, t1/2=1.2h
dsRNA, t1/2=n.d. (>10h)
GADD34 mRNA (%)
Actinomycin D (h)
C
DMSO, t1/2=1.3h
Thap 1h, **** t1/2=n.d.(>10h)
Thap 3h, **** t1/2=4.5h
Thap 6h, ** t1/2=2.9h
Thap 12h, ** t1/2=2.4h
GADD34 mRNA (%)
Actinomycin D (h)
D
GADD34 3'UTR:
AU-rich element (ARE)
AUUUA pentamer
AAUAAA polyA signal
WT 5'-GACCAACUGGUUUGCCUAUAAUUUUAUUAACUAUUUUAUUUUUUCUAAGUGUGGGUUUAUAUAAGGAAUAAAGCCUUUUGAUUUGUA-3'
MUT 5'-GACCAACUGGUUUGCCUAUAAUGUAUUAACUAUGUAUUUUUUCUAAGUGUGGGUUUAUAUAAGGAAUAAAGCCUUUUGAUUUGUA-3'
E
Wildtype (WT)
TNF-α ARE
GADD34 3'UTR
GADD34MUT 3'UTR
β-globin
3'UTR
AREs
G G
(A)n
F
WT, t1/2=12.3h
TNF-α, t1/2=2.5h ****
GADD34, t1/2=2.9h ****
GADD34MUT, t1/2=8.3h n.s.
β-globin mRNA (%)
Actinomycin D (h)
G
GADD34 mRNA level (fold GAPDH)
n.s.
Ctrl
ΔARE
H
Ctrl cls
ΔARE cls
GADD34 mRNA expr. (fold DMSO)
n.s.
**
Thapsigargin treatment (h)
I
Ctrl, t1/2=0.9h
ΔARE, t1/2=1.2h
DMSO
Ctrl, t1/2=n.d. (>10h)
ΔARE, t1/2=n.d. (>10h)
1h Thap
Ctrl, t1/2=1.7h
ΔARE, t1/2=n.d. (>10h)
3h Thap
Ctrl, t1/2=2.0h
ΔARE, t1/2=3.0h
6h Thap
GADD34 mRNA (%)
Actinomycin D (h)

**Figure 2**

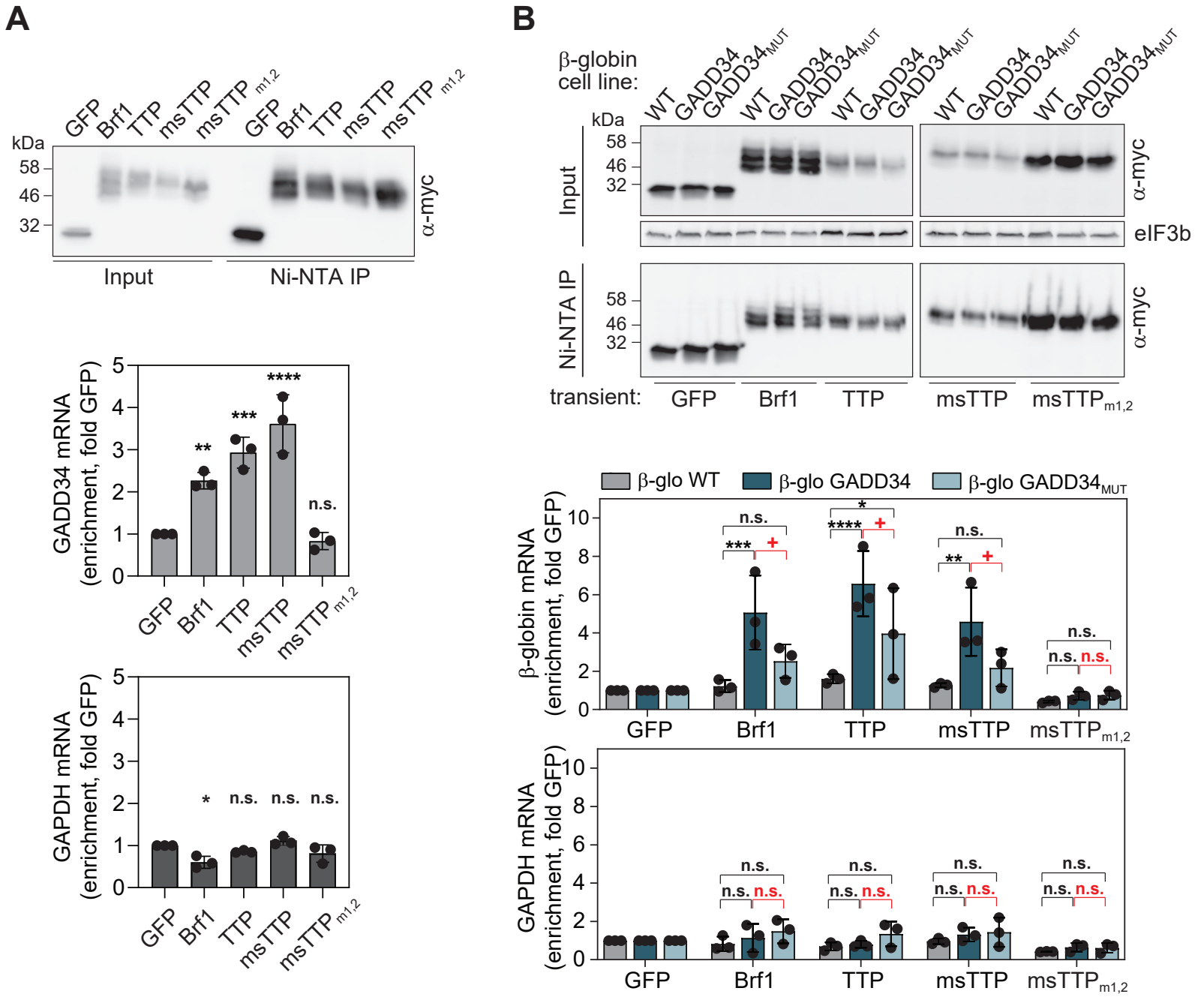
A
GFP
Brf1
TTP
msTTP
msTTP m1,2
kDa
58
46
32
α-myc
Input
Ni-NTA IP
GADD34 mRNA (enrichment, fold GFP)
**
***
****
n.s.
GAPDH mRNA (enrichment, fold GFP)
*
n.s.
B
β-globin cell line:
WT
GADD34
GADD34MUT
Input
Ni-NTA IP
eIF3b
transient:
msTTPm1,2
β-glo WT
β-glo GADD34
β-glo GADD34MUT
β-globin mRNA (enrichment, fold GFP)
+

**Figure 3**

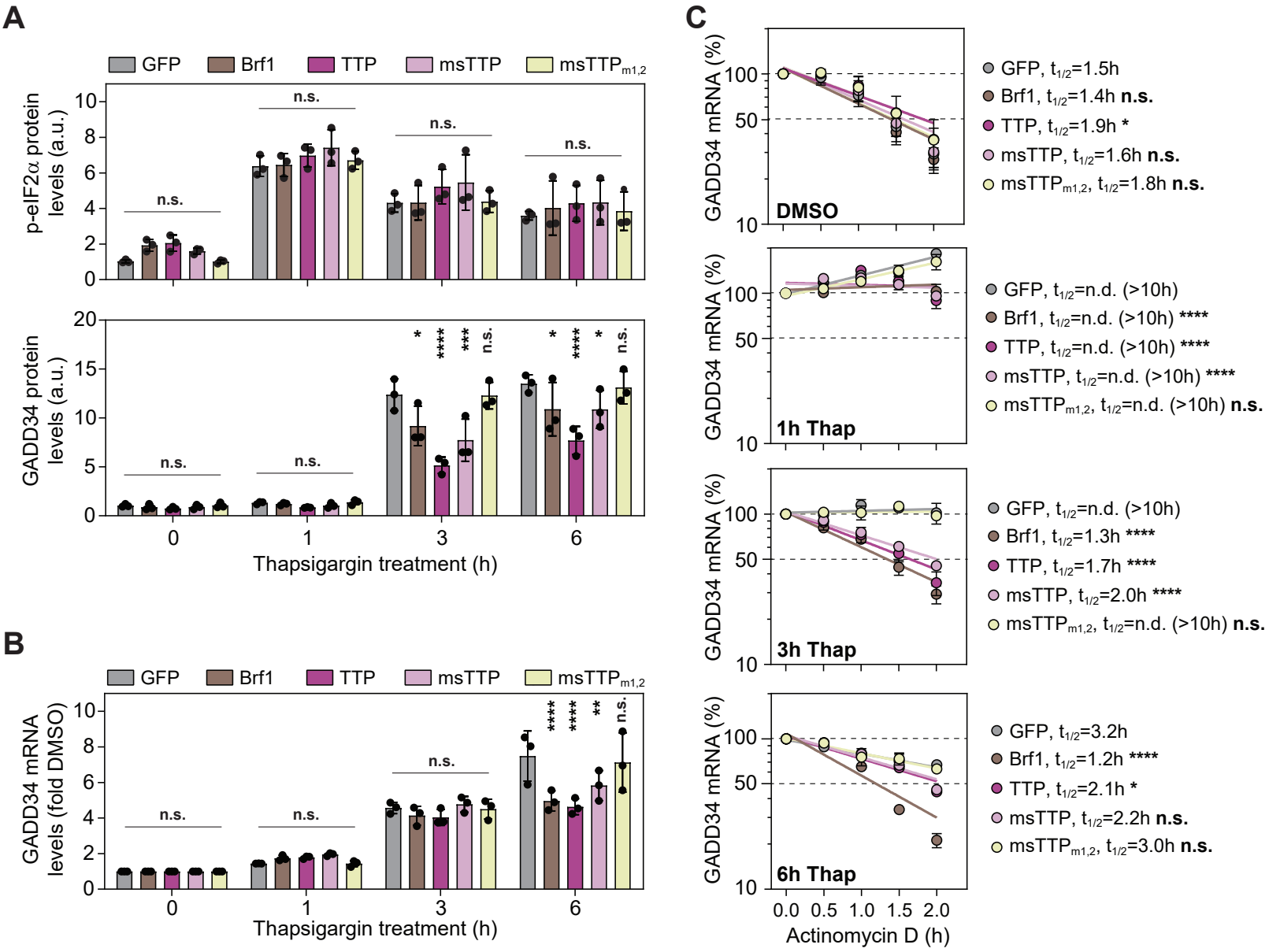
A
GFP
Brf1
TTP
msTTP
msTTPm1,2
p-eIF2α protein levels (a.u.)
n.s.
GADD34 protein levels (a.u.)
*
****
***
Thapsigargin treatment (h)
B
GADD34 mRNA levels (fold DMSO)
**
C
GADD34 mRNA (%)
DMSO
GFP, t1/2=1.5h
Brf1, t1/2=1.4h n.s.
TTP, t1/2=1.9h *
msTTP, t1/2=1.6h n.s.
msTTPm1,2, t1/2=1.8h n.s.
1h Thap
GFP, t1/2=n.d. (>10h)
Brf1, t1/2=n.d. (>10h) ****
TTP, t1/2=n.d. (>10h) ****
msTTP, t1/2=n.d. (>10h) ****
msTTPm1,2, t1/2=n.d. (>10h) n.s.
3h Thap
Brf1, t1/2=1.3h ****
TTP, t1/2=1.7h ****
msTTP, t1/2=2.0h ****
6h Thap
GFP, t1/2=3.2h
Brf1, t1/2=1.2h ****
TTP, t1/2=2.1h *
msTTP, t1/2=2.2h n.s.
msTTPm1,2, t1/2=3.0h n.s.
Actinomycin D (h)

# Figure 4

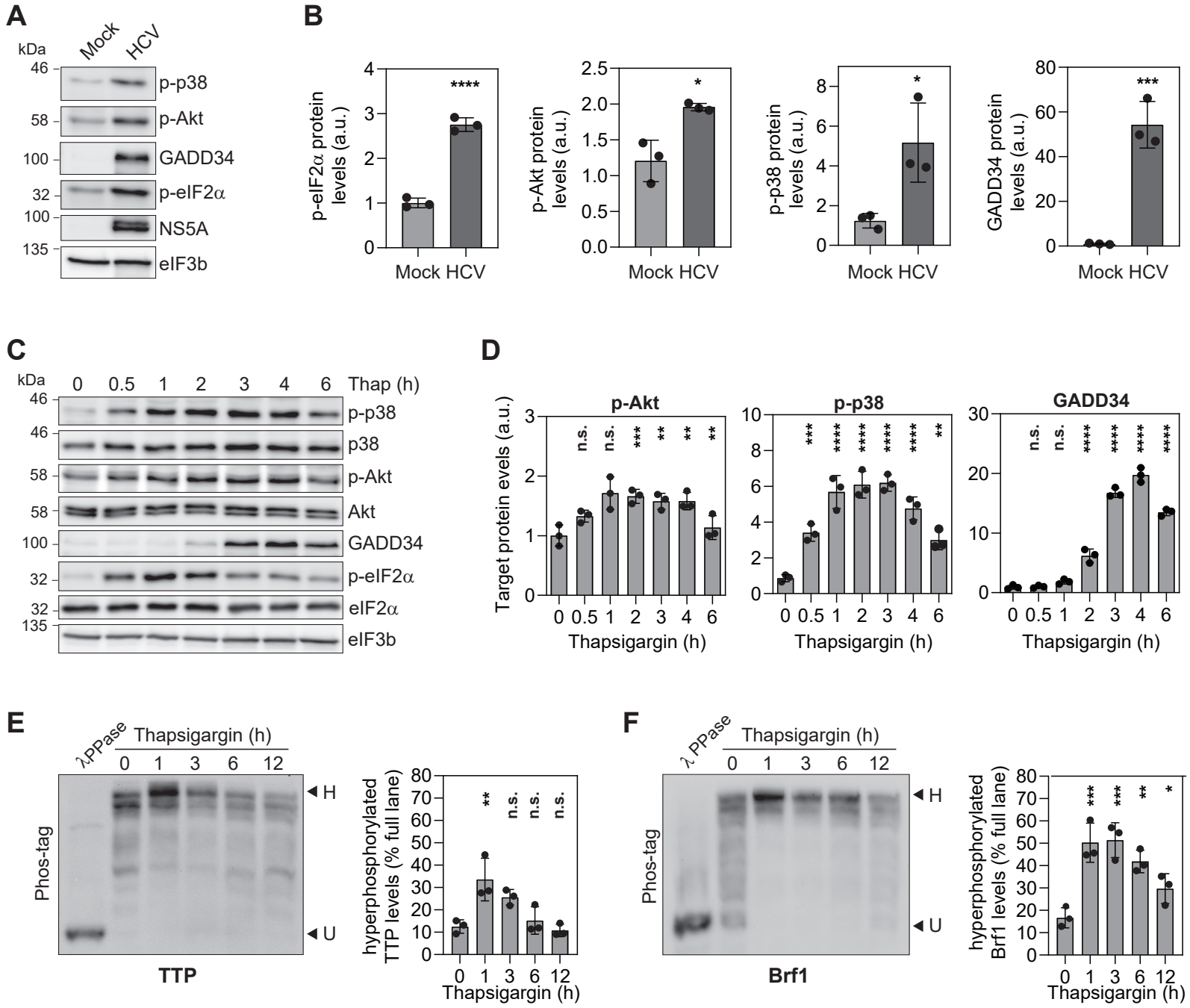
A
kDa
Mock
HCV
46
p-p38
58
p-Akt
100
GADD34
32
p-eIF2α
100
NS5A
135
eIF3b
B
p-eIF2α protein levels (a.u.)
p-Akt protein levels (a.u.)
p-p38 protein levels (a.u.)
GADD34 protein levels (a.u.)
Mock HCV
C
kDa
0 0.5 1 2 3 4 6 Thap (h)
p-p38
p38
p-Akt
Akt
GADD34
p-eIF2α
eIF2α
eIF3b
D
p-Akt
p-p38
GADD34
Target protein evels (a.u.)
n.s.
Thapsigargin (h)
E
λPPase
Thapsigargin (h)
0 1 3 6 12
Phos-tag
H
U
TTP
hyperphosphorylated TTP levels (% full lane)
F
λ PPase
Brf1
hyperphosphorylated Brf1 levels (% full lane)

# Figure 5

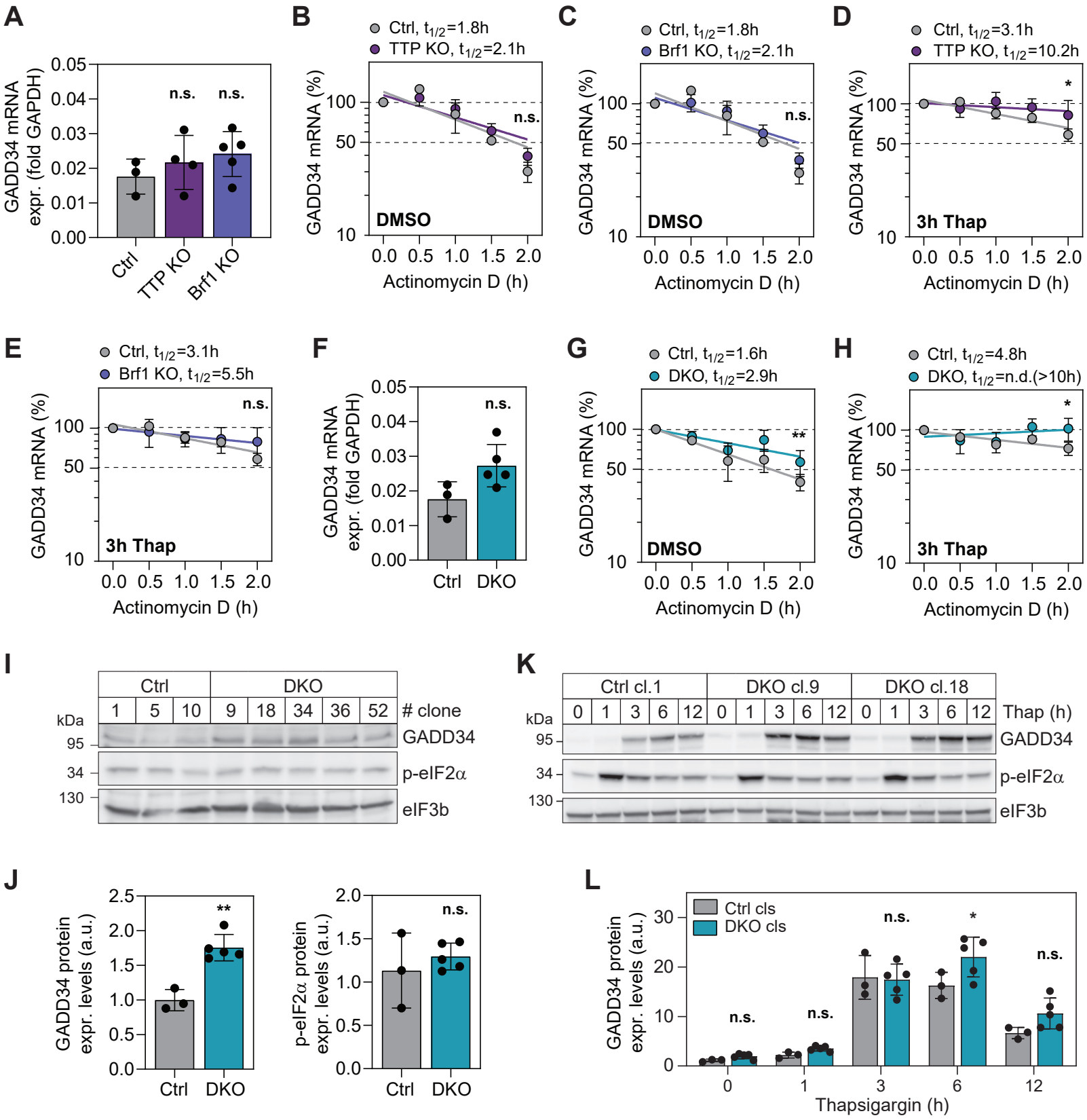
A
GADD34 mRNA expr. (fold GAPDH)
0.05
0.04
0.03
0.02
0.01
0.00
n.s.
n.s.
Ctrl
TTP KO
Brf1 KO
B
Ctrl, t1/2=1.8h
TTP KO, t1/2=2.1h
GADD34 mRNA (%)
100
50
10
n.s.
DMSO
0.0 0.5 1.0 1.5 2.0
Actinomycin D (h)
C
Ctrl, t1/2=1.8h
Brf1 KO, t1/2=2.1h
GADD34 mRNA (%)
100
50
10
n.s.
DMSO
0.0 0.5 1.0 1.5 2.0
Actinomycin D (h)
D
Ctrl, t1/2=3.1h
TTP KO, t1/2=10.2h
GADD34 mRNA (%)
100
50
10
*
3h Thap
0.0 0.5 1.0 1.5 2.0
Actinomycin D (h)
E
Ctrl, t1/2=3.1h
Brf1 KO, t1/2=5.5h
GADD34 mRNA (%)
100
50
10
n.s.
3h Thap
0.0 0.5 1.0 1.5 2.0
Actinomycin D (h)
F
GADD34 mRNA expr. (fold GAPDH)
0.05
0.04
0.03
0.02
0.01
0.00
n.s.
Ctrl
DKO
G
Ctrl, t1/2=1.6h
DKO, t1/2=2.9h
GADD34 mRNA (%)
100
50
10
**
DMSO
0.0 0.5 1.0 1.5 2.0
Actinomycin D (h)
H
Ctrl, t1/2=4.8h
DKO, t1/2=n.d.(>10h)
GADD34 mRNA (%)
100
50
10
*
3h Thap
0.0 0.5 1.0 1.5 2.0
Actinomycin D (h)
I
Ctrl
DKO
1 5 10 9 18 34 36 52
# clone
kDa
95
GADD34
34
p-eIF2α
130
eIF3b
K
Ctrl cl.1
DKO cl.9
DKO cl.18
0 1 3 6 12 0 1 3 6 12 0 1 3 6 12
Thap (h)
kDa
95
GADD34
34
p-eIF2α
130
eIF3b
J
GADD34 protein expr. levels (a.u.)
2.5
2.0
1.5
1.0
0.5
0.0
**
Ctrl
DKO
p-eIF2α protein expr. levels (a.u.)
2.0
1.5
1.0
0.5
0.0
n.s.
Ctrl
DKO
L
Ctrl cls
DKO cls
GADD34 protein expr. levels (a.u.)
30
20
10
0
n.s.
n.s.
n.s.
*
n.s.
0
1
3
6
12
Thapsigargin (h)

Figure 6

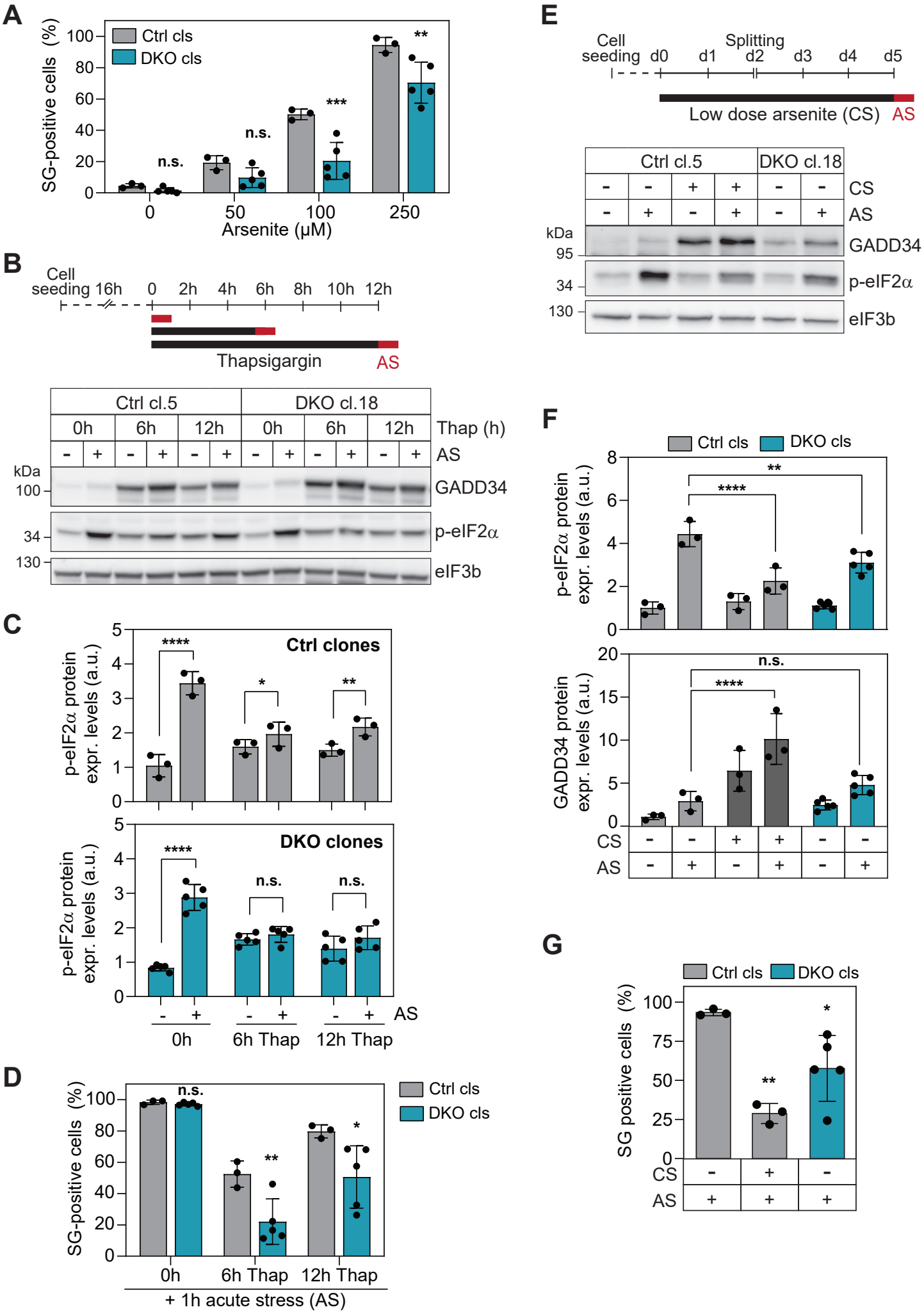
A
SG-positive cells (%)
Ctrl cls
DKO cls
n.s.
n.s.
***
**
Arsenite (μM)
B
Cell seeding 16h
0 2h 4h 6h 8h 10h 12h
Thapsigargin
AS
Ctrl cl.5
DKO cl.18
0h 6h 12h 0h 6h 12h
Thap (h)
AS
kDa
GADD34
p-eIF2α
eIF3b
C
Ctrl clones
DKO clones
p-eIF2α protein expr. levels (a.u.)
****
*
**
n.s.
0h
6h Thap
12h Thap
D
SG-positive cells (%)
Ctrl cls
DKO cls
+ 1h acute stress (AS)
E
Cell seeding
Splitting
d0 d1 d2 d3 d4 d5
Low dose arsenite (CS)
CS
F
GADD34 protein expr. levels (a.u.)
G
SG positive cells (%)

Figure 7

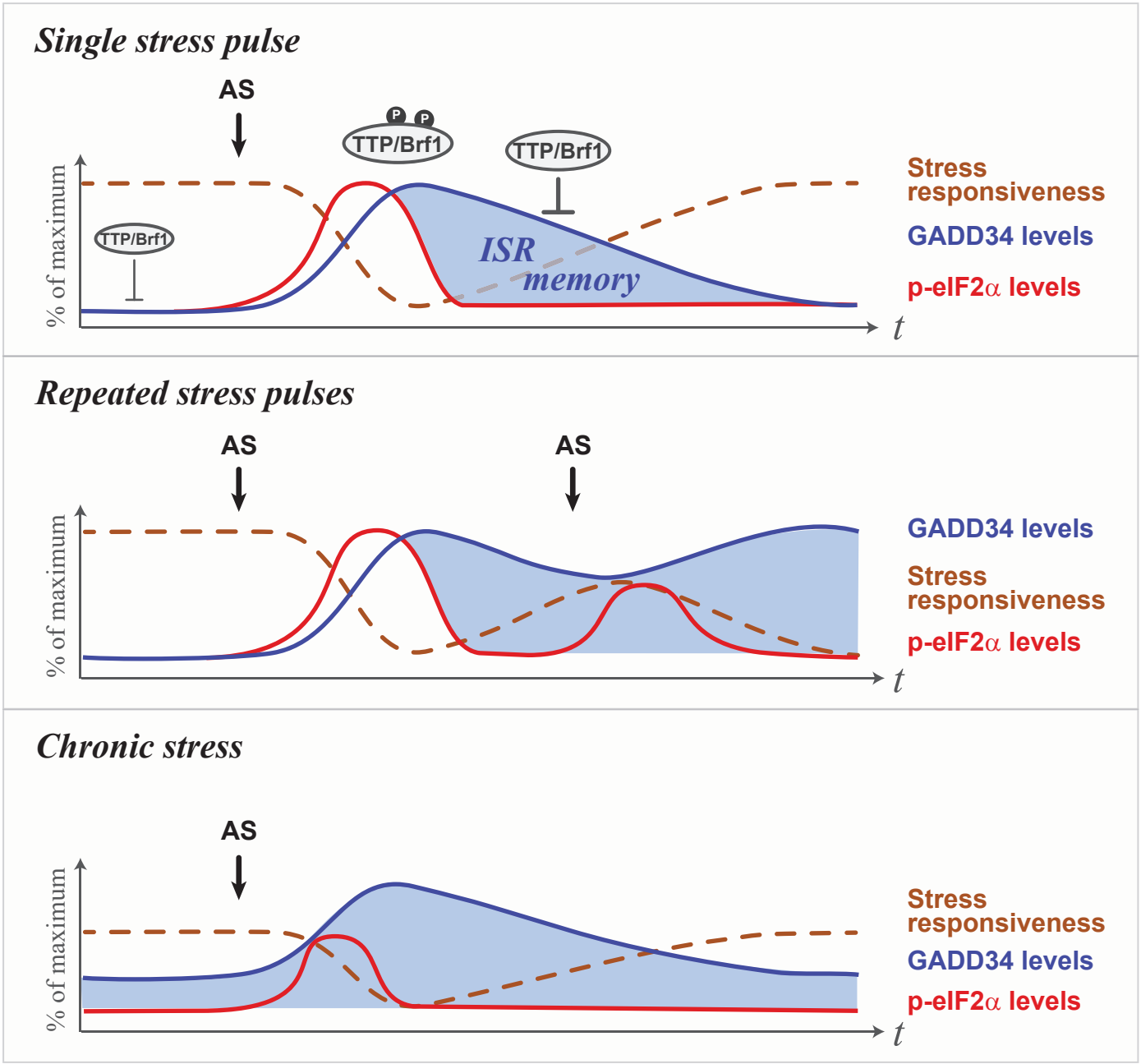
Single stress pulse
AS
TTP/Brf1
P
P
TTP/Brf1
TTP/Brf1
% of maximum
ISR
memory
Stress responsiveness
GADD34 levels
p-eIF2α levels
t
Repeated stress pulses
AS
AS
% of maximum
GADD34 levels
Stress responsiveness
p-eIF2α levels
t
Chronic stress
AS
% of maximum
Stress responsiveness
GADD34 levels
p-eIF2α levels
t

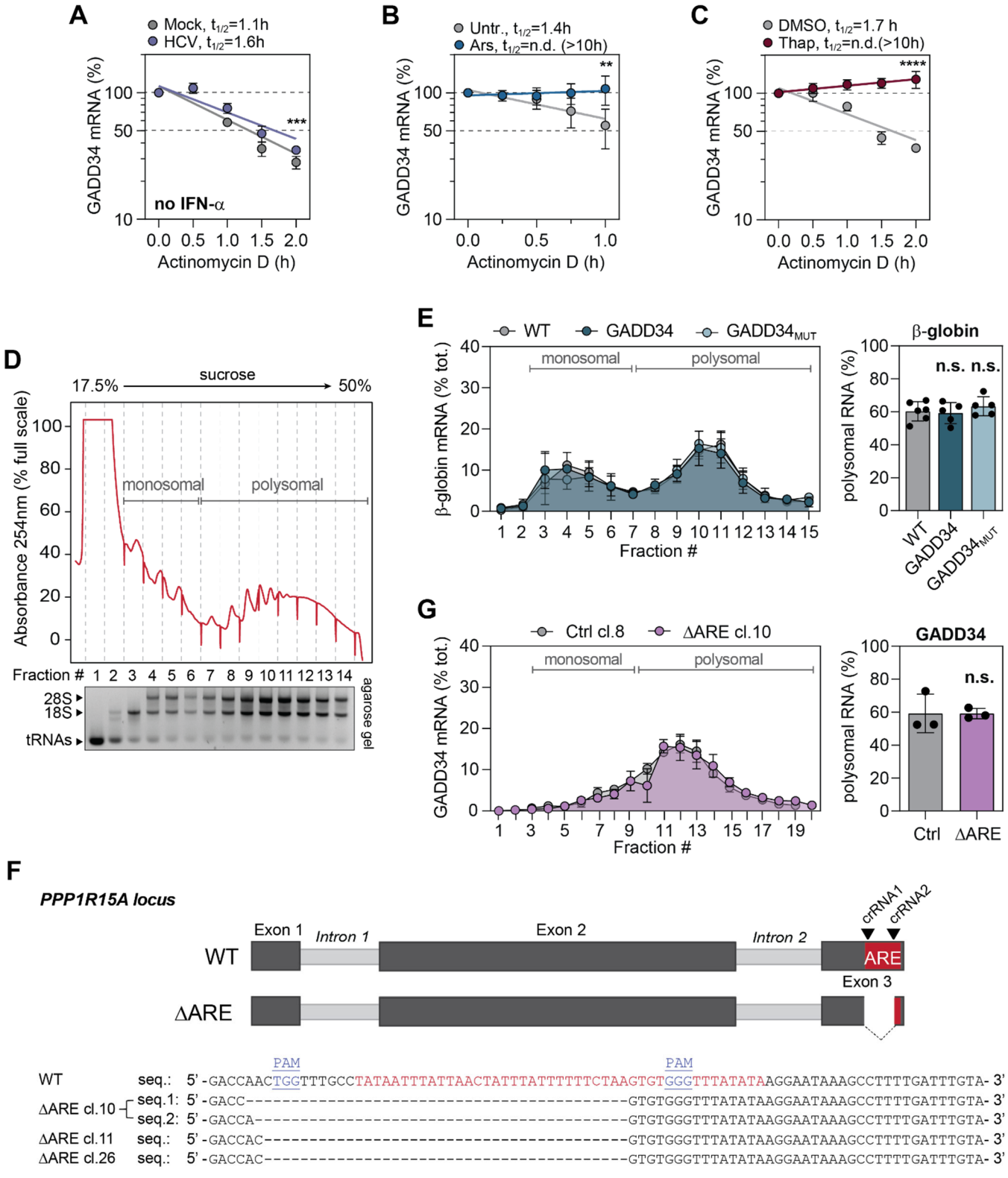


**Figure S1. GADD34 ARE regulates mRNA stability, but not translation efficiency (related to Figure 1). (A)** GADD34 mRNA decay in cells infected with HCV for 48 h prior to actinomycin D chase. Levels of GADD34 were determined by qRT-PCR, normalized to stable GAPDH transcripts and plotted as percentage of the initial time point. GADD34 mRNA half-lives ($t_{1/2}$) were calculated using a semi-logarithmic curve fitting. Shown are means ± SD of

biological replicates (n=3). **(B)** GADD34 mRNA decay in cells were treated with sodium arsenite for 30 min prior to actinomycin D chase. Analysis as in (A). Shown are means ± SD of biological replicates (n=3). **(C)** GADD34 mRNA decay after 1 hour treatment with thapsigargin (Thap). Analysis as in (A). Shown are means ± SD of biological replicates (n=3). **(D and E)** Analysis of β-globin reporter mRNA translation efficiency using polysome profiling. (D) Representative polysome profile. After separation by ultra-centrifugation, sucrose gradients were eluted from the top using a fractionator and absorption at 254 nm was continuously recorded (upper panel). Fractions were collected (#1 to 14), total RNA was extracted and analyzed by agarose gel electrophoresis (lower panel) to confirm the presence of 18S and 28S ribosomal RNA. (E) Abundance of specific mRNAs in each fraction was analyzed by qRT-PCR. Left panel shows the percentage of β-globin reporter mRNA (WT, GADD34 or $GADD34_{MUT}$) in individual fractions. Right panel shows the percentage of each mRNA in total polysomal RNA. Shown are means ± SD of independent biological repeats, β-glo WT (n=6), GADD34 (n=5) or $GADD34_{MUT}$ (n=5). **(F)** GADD34ΔARE validation by sequencing. The upper panel depicts the knockout strategy. AU-rich element (ARE) was deleted using CRISPR-Cas9 and a combination of two crRNAs targeting *PPP1R15A* exon 3. Single cell clones were selected and the deletion of the genomic sequence between the guide RNAs (PAM motifs are indicated in blue) confirmed by sequencing. **(G)** Polysome profile analyses of representative Ctrl #8 and GADD34ΔARE #10 cell clones. Analysis as in (E). Shown are mean ± SD of biological repeats (n=3). Distribution of GADD34 mRNA in the gradient fractions (left panel) and percentage of total polysomal RNA (right panel).

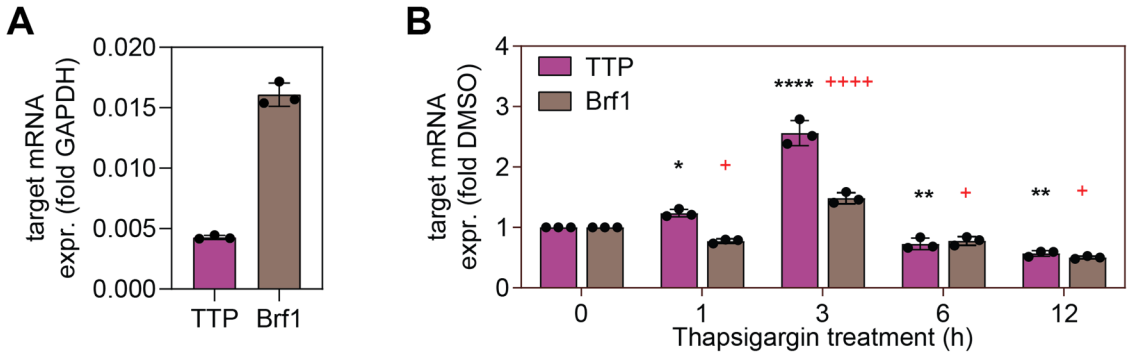


**Figure S2. Variation of TTP and BRF1 expression during long periods of stress (related to Figure 2). (A)** Relative mRNA expression of TTP and Brf1 in Huh7 cells under normal conditions. Values were normalized to GAPDH mRNA levels. Shown are means ± SD (n=3). **(B)** Relative mRNA expression of TTP and Brf1 in cells treated with thapsigargin for the indicated times or solvent control (0 h). Values were normalized to GAPDH mRNA levels and shown as fold solvent control (0 h). Shown are means ± SD (n=3). *, statistical significance compared to TTP mRNA levels at T0. +, statistical significance compared to Brf1 mRNA levels at T0.

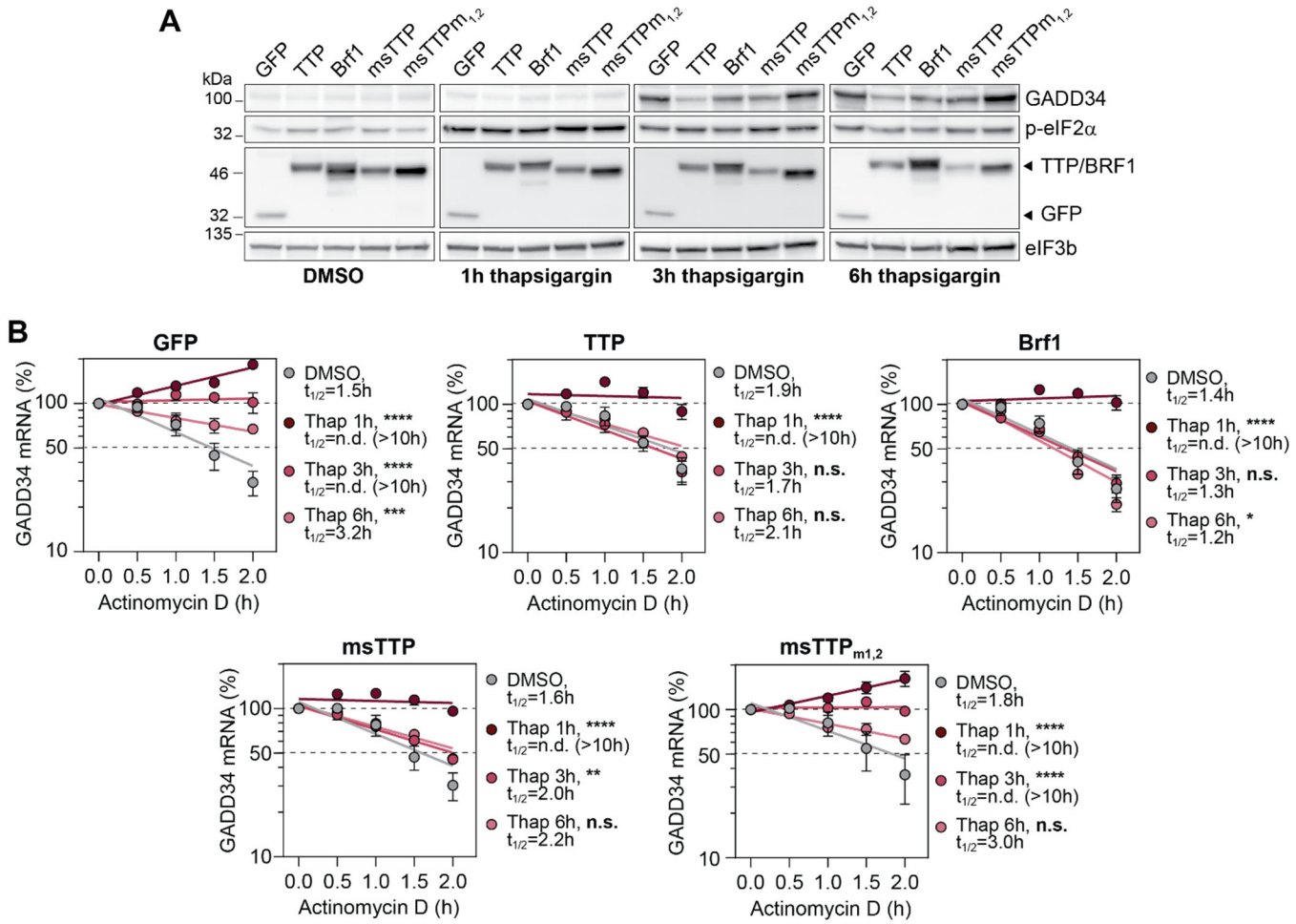


**Figure S3. TTP and Brf1 overexpression interferes with GADD34 mRNA stabilization upon acute stress induction (related to Figure 3). (A)** Expression of GADD34 and p-eIF2α in cells transiently expressing myc-his tagged proteins, treated with thapsigargin for the indicated times or with solvent control (0 h). Shown is a representative Western blot analysis (n=3). **(B)** GADD34 mRNA decay in cells transiently expressing myc-his tagged proteins and treated with thapsigargin for the indicated times or solvent control (DMSO) prior to actinomycin D chase. The original data depicted here is identical with Figure 3C. Shown are mean ± SD (n=3). Statistical significance over all time points compared to DMSO is indicated.

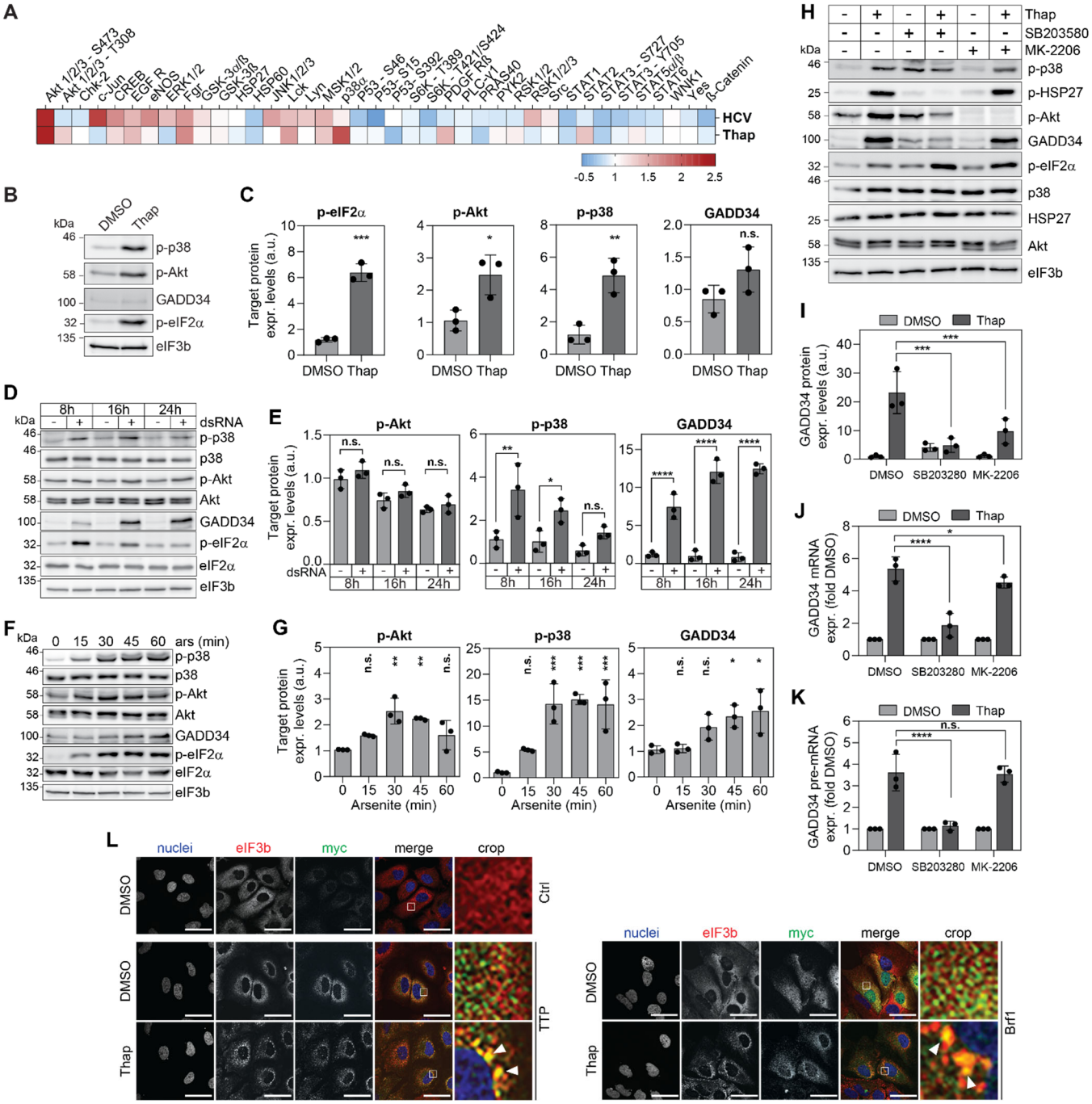


**Figure S4. Transient activation of the p38-MAPK/MK2 and PI3K/Akt signaling pathways upon stress (related to Figure 4). (A)** The phosphorylation levels of several human MAPK kinases were measured using the human phospho-MAPK array in response to HCV infection in the presence of IFN-α or in response to thapsigargin. Cells treated with IFN-α or with DMSO served as control, respectively. The heat map depicts changes in kinase phosphorylation levels compared to controls. Shown are means of independent biological replicates (n=3). Color gradient indicate fold changes compared to the corresponding controls. **(B and C)** Analysis of p38-MAPK/MK2 and PI3K/Akt signaling pathways in cells treated with thapsigargin or solvent control (DMSO) for 1 h (n=3). (B) Representative Western blot analysis. (C) Quantifications of protein abundance corresponding to *(c)*. Measured band intensities were normalized to loading control (eIF3b) and are depicted as arbitrary units (a.u.). Shown are means ± SD. Statistical significance compared to DMSO is indicated. **(D to G)** Activation of the p38-MAPK/MK2

and PI3K/Akt signaling pathways in response to different stressors. (D) Representative Western blot analysis of cells transfected with dsRNA (n=3). (E) Quantification corresponding to (D). Statistical significance compared to non-transfected controls of each time point is indicated. (F) Representative Western blot analysis of cells treated with arsenite (n=3). (G) Quantification corresponding to (F). Statistical significance compared to T0 is indicated. **(H to K).** Stress-induced expression of GADD34 is p-p38 and p-Akt dependent**.** Inhibition of p38-MAPK/MK2 and PI3K/Akt signaling pharmacological inhibitors. Cells were pre-treated with SB203580, an inhibitor p38-MAPK catalytic activity, or MK-2206, a pan Akt inhibitor, for 1 h prior to the addition of thapsigargin or DMSO. Samples were harvested at 3 h post stress exposure. (H) Pathway analysis. Basal and phosphorylated forms of p38, Akt, eIF2$\alpha$ and HSP27, a downstream target of p38, were measured. Shown is a representative Western blot analysis (n=3). (I) Quantifications corresponding to (I). Measured band intensities were normalized to loading control (eIF3b) and are depicted as arbitrary units (a.u.). Statistical significance of thapsigargin compared to DMSO-treated cells is indicated. Measurement of GADD34 mRNA (J) and pre-mRNA levels (K) by qRT-PCR. Values were normalized to GAPDH values and are shown as fold DMSO control. Shown are means ± SD (n=3). Statistical significance of thapsigargin compared to DMSO-treated cells is indicated. **(L)** Immunofluorescence analysis of myc-his TTP and Brf1 localization in cells treated with thapsigargin or solvent control (DMSO) for 1 h (n=3). Cells were fixed and stained using a myc-tag specific antibody to determine TTP and Brf1 (green), eIF3b antibody to visualize SGs (green) and DAPI to visualize nuclei (blue). Confocal micrographs show representative maximum-intensity of Z-projections of 3 focal planes. Scale bar, 50 μM. The region in the white squares is shown as cropped section on the right. Arrowheads indicate colocalization

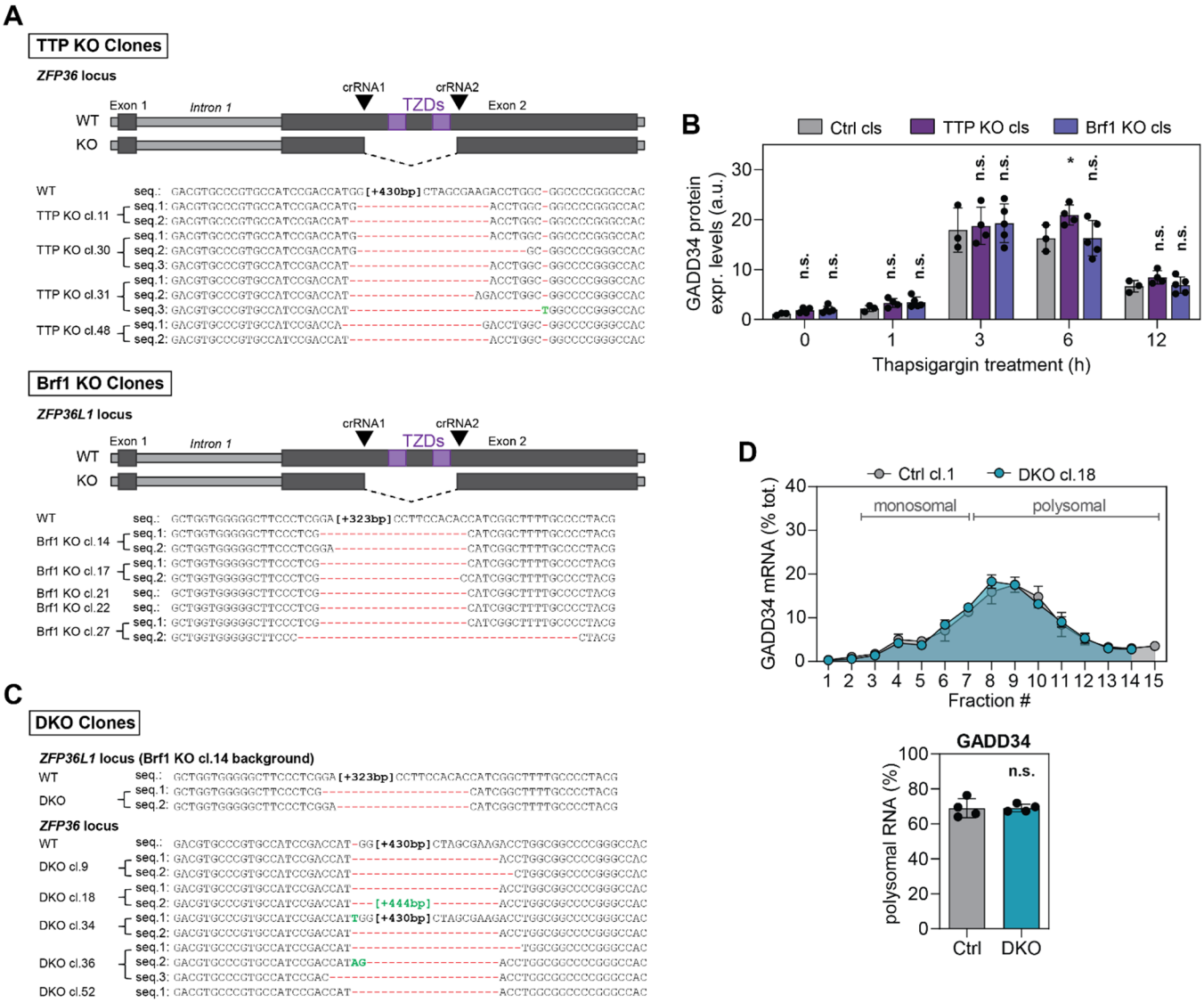


**Figure S5. Characterization of TTP and Brf1 single and double KO cell clones (related to Figure 5). (A)** KO cell clones were generated CRISPR/Cas9 approach and using two guide RNAs (crRNA1 and crRNA2) to delete the region containing the TZF domains (TZDs) in exon 2 of the TTP gene locus *ZFP36* and the Brf1 gene locus *ZFP36L1*. Homozygous KO clones were selected based on their genomic DNA sequence. Sequences of individual alleles (up to three) for each clone are indicated. Nucleotide deletions are indicated by red dashes, insertions are marked in green. **(B)** Quantification of GADD34 protein expression levels in Ctrl (n=3), TTP KO (n=4) and Brf1 KO (n=5) cells after exposure to thapsigargin. Cell clones were treated with thapsigargin for the indicated times or with solvent control (T0) (n = 2). Measured band intensities were normalized to loading control (eIF3b) and are depicted as arbitrary units (a.u.). Shown are representative means of cell clones ± SD. Statistical significance compared to Ctrl clones for each time point is indicated. **(C)** DKO cell lines were generated by deleting TTP TZD genomic region in Brf1 single KO cell clone #14. Homozygous KO clones were selected based on their genomic DNA sequence. Sequences of individual alleles (up to three) for each clone are indicated. Nucleotide deletions are marked by red dashes, insertions are marked in green. **(D)** Polysome profile analysis of representative Ctrl cell clone (#1) and DKO cell clone #18. GADD34 mRNA levels were analyzed by qRT-PCR. Left panel shows the percentage of GADD34 mRNA in each fraction relative to total amount of GADD34 mRNA in the gradient. Right panel shows the percentage of polysomal GADD34 mRNA compared to total RNA. Shown are means ± SD of independent biological repeats (n=4).

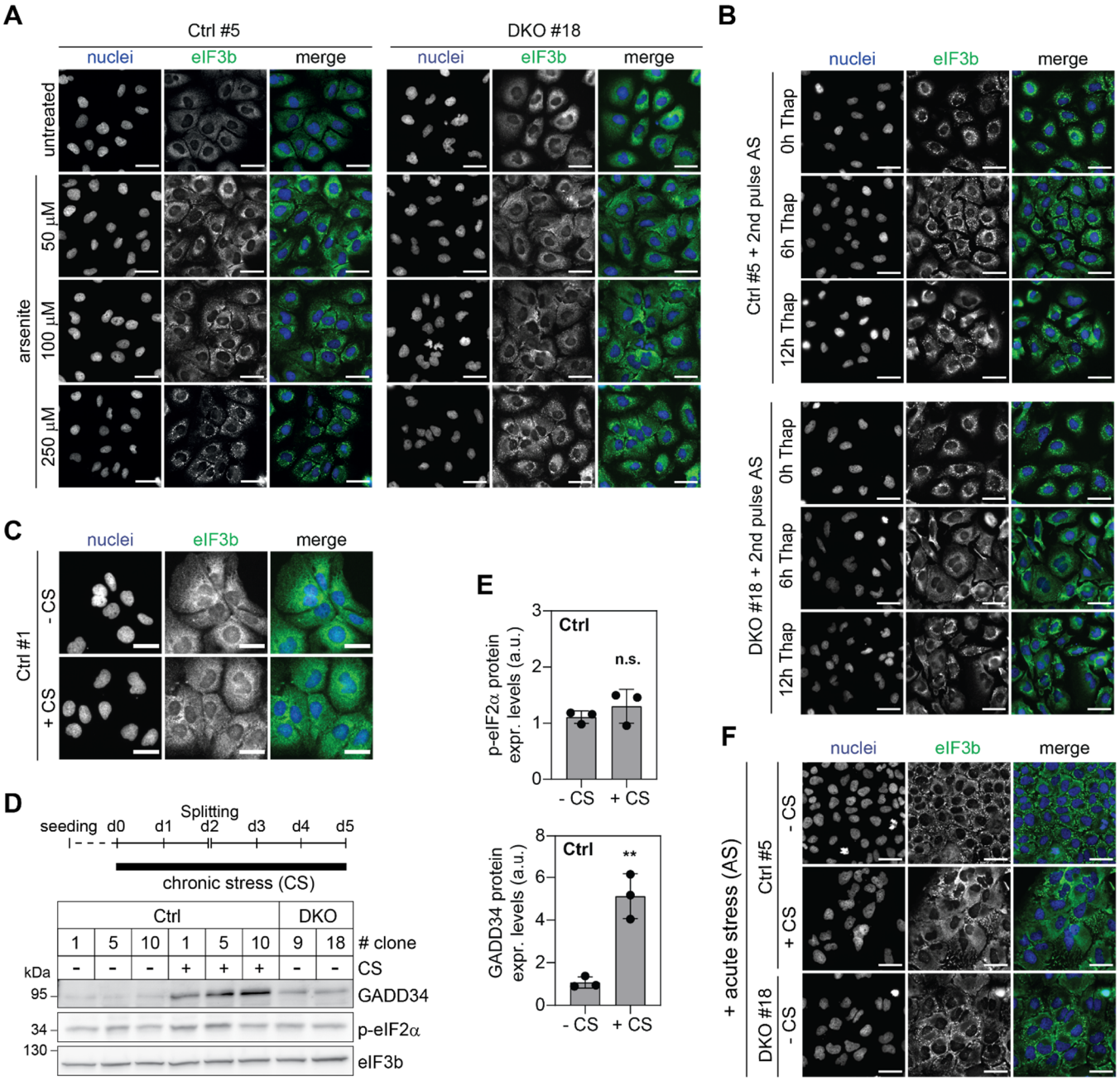


**Figure S6. Reduced stress responsiveness in DKO cell clones (related to Figure 6). (A)** Immunofluorescence analysis of SG formation in Ctrl and DKO cell clones treated with increasing concentrations of arsenite. Cells were fixed and stained for nuclei (blue), and eIF3b (green) as SG marker. Shown are representative immunofluorescence images for Ctrl cell clone #5 and DKO cell clone #18. Scale bar, 50 µm. **(B)** SG formation in Ctrl and DKO cell clones treated with thapsigargin for 6 or 12 h prior to exposure to an acute pulse of sodium arsenite for 45 min (AS) (n=2). Cells were fixed and stained for nuclei (blue), and eIF3b (green) as SG marker. Shown are representative immunofluorescence images for Ctrl cell clone #5 and DKO cell clone #18. Scale bar, 50 µm. **(C)** SG formation in Ctrl cell clones maintained for 5 days in the presence of low-dose arsenite (chronic stress, CS). Cells maintained in the absence of arsenite (no CS) for the same duration were used as control. Shown are representative immunofluorescence images for Ctrl cell clone #1. Cells were fixed and stained for nuclei (blue), and eIF3b (green) as SG marker. Scale bar, 50 µm. **(D)** The upper panel shows the schematic of the experimental design. The lower panel shows a representative Western blot analysis of GADD34 and p-eIF2α expression in chronically stressed Ctrl

cell clones compared to basal levels of two DKO individual cell clones #9 and #18 (n=2). **(E)** Quantifications corresponding to (D). Measured band intensities were normalized to loading control (eIF3b) and are depicted as arbitrary units (a.u.). Shown is a representative mean protein abundance ± SD in all individual Ctrl cell clones in the presence (+CS) or absence of chronic stress (-CS) (n=2). Statistical significance compared to Ctrl clones in absence of CS in indicated. **(F)** At day 5, cells were challenged with a second pulse of 50 µM arsenite (AS) for 45 min before harvest (n=2). Shown are representative immunofluorescence images for Ctrl cell clone #5. DKO cell clone #18 served as comparison. Scale bar, 50 µm.